Earth-Science Reviews 221 (2021) 103769

Contents lists available at ScienceDirect

Earth-Science Reviews

journal homepage: www.elsevier.com/locate/earscirev

Review Article

OSL-dating of the Pleistocene-Holocene climatic transition in loess from China, Europe and North America, and evidence for accretionary pedogenesis

D. Constantin [a,b,*], J.A. Mason [c], D. Veres [d], U. Hambach [e], C. Panaiotu [f], C. Zeeden [g], L. Zhou [h], S. B. Marković [i], N. Gerasimenko [j], A. Avram [a,k], V. Tecsa [a,k], S.M. Groza-Sacaciu [a,k], L. del Valle Villalonga [a,k], R. Begy [a,b,k], A. Timar-Gabor [a,b,k]

[a] Institute for Interdisciplinary Research in Bio-Nano-Sciences, Babeş-Bolyai University, Treboniu Laurian 42, 400271 Cluj-Napoca, Romania
[b] Institute "Emil G. Racoviță" for research on extreme life conditions, Babeş-Bolyai University, Treboniu Laurian 42, 400271 Cluj-Napoca, Romania
[c] Department of Geography, University of Wisconsin-Madison, 550 North Park ST, Madison, WI 53706, USA
[d] Romanian Academy, Institute of Speleology, Clinicilor 5, 400006 Cluj-Napoca, Romania
[e] BayCEER & Chair of Geomorphology, University of Bayreuth, 94450 Bayreuth, Germany
[f] Physics Faculty, University of Bucharest, Bălcescu 1, 010041 Bucharest, Romania
[g] LIAG, Leibniz Institute for Applied Geophysics, Stilleweg 2, Hannover 30655, Germany
[h] Key Laboratory for Earth Surface Processes, Department of Geography, Peking University, Beijing 100871, China
[i] Laboratory for Paleoenvironmental Reconstruction, Faculty of Sciences, University of Novi Sad, Trg Dositeja Obradovića 3, 21000 Novi Sad, Serbia
[j] Earth Sciences and Geomorphology Department, Taras Shevchenko National University of Kyiv, Glushkova Prospect 2a, 03127 Kiev, Ukraine
[k] Faculty of Environmental Sciences and Engineering, Babeş-Bolyai University, Fântânele 30, 400327 Cluj-Napoca, Romania

ARTICLE INFO

Keywords:
Accretional soils
Pleistocene-Holocene transition
Luminescence dating
Quartz
Magnetic susceptibility

ABSTRACT

Loess deposits intercalated by paleosols are detailed terrestrial archives of Quaternary climate variability providing information on the global dust cycle and landscape dynamics. Their paleoclimatic significance is often explored by quantifying their mineral magnetic properties due to their sensitivity to local/regional hydroclimate variability. Detailed chronological assessment of such regional proxy records around the climatic transitions allow a better understanding of how regional records react to major global climatic transitions such as the Pleistocene-Holocene climatic transition.

Logs of high-resolution magnetic susceptibility and its frequency dependence were used as paleoclimatic proxies to define the environmental transition from the last glacial loess to the current interglacial soil as reflected in nine loess-paleosol sequences across the northern hemisphere, from the Chinese Loess Plateau, the southeastern European loess belt and the central Great Plains, USA. The onset of increase in magnetic susceptibility above typical loess values was used to assess the onset of, and developments during, the Pleistocene-Holocene climatic transition.

High-resolution luminescence dating was applied on multiple grain-sizes (4–11 μm, 63–90 μm, 90–125 μm) of quartz extracts from the same sample in order to investigate the timing of Pleistocene-Holocene climatic transition in the investigated sites.

The magnetic susceptibility signal shows a smooth and gradual increase for the majority of the sites from the typical low loess values to the interglacial ones. The initiation of this increase, interpreted as recording the initiation of the Pleistocene-Holocene climatic transition at each site, was dated to 14–17.5 ka or even earlier. Our chronological results highlight the need of combining paleoclimatic proxies (magnetic susceptibility) with absolute dating when investigating the Pleistocene-Holocene climatic transition as reflected by the evolution of this proxy in order to avoid chronostratigraphic misinterpretations in loess-paleosol records caused by simple pattern correlation.

The detailed luminescence chronologies evidence the continuity of eolian mineral dust accumulation regardless of glacial or interglacial global climatic regimes. Coupled with magnetic susceptibility records this

* Corresponding author at: Institute for Interdisciplinary Research in Bio-Nano-Sciences, Babeş-Bolyai University, Treboniu Laurian 42, 400271 Cluj-Napoca, Romania.
E-mail address: daniela.constantin@ubbcluj.ro (D. Constantin).

https://doi.org/10.1016/j.earscirev.2021.103769
Received 4 March 2021; Received in revised form 5 August 2021; Accepted 10 August 2021
Available online 12 August 2021

indicates that dust sedimentation and pedogenesis act simultaneously and result in a non-negligible accretional component in the formation of Holocene soils in loess regions across the Northern Hemisphere. The luminescence ages allowed the modeling of accumulation rates for the Holocene soil which are similar for European, Chinese and U.S.A. loess sites investigated and vary from 2 cm ka^{-1} to 9 cm ka^{-1}. While accretional pedogenesis has often been implicitly or explicitly assumed in paleoclimatic interpretation of loess-paleosol sequences, especially in the Chinese Loess Plateau, our luminescence data add direct evidence for ongoing sedimentation as interglacial soils formed.

1. Introduction

Loess-paleosol sequences (LPS) are mostly distributed across the mid-latitudes forming the loess belt of the Northern Hemisphere. They are considered quasi-continuous terrestrial archives of Quaternary climate variability providing information on the global dust cycle and landscape dynamics (Schaetzl et al., 2018; Lehmkuhl et al., 2021). The characteristic alternations of loess and paleosol horizons reflect the climatic fluctuation between relatively dry-cool and warm-humid conditions linked to glacial-interglacial climate variability. Their timing is often assumed synchronous with major trends in climate variability documented in marine and ice core records (Bazin et al., 2013; Govin et al., 2015) to which LPS are often matched on an orbital scale of past climate variability (Marković et al., 2015; Zeeden et al., 2020).

Well known interactions between atmosphere – biosphere – pedosphere documented in other paleoclimatic records (Clark et al., 2012; Stern and Lisiecki, 2014; Magyari et al., 2019) highlight the need for well-dated, high-resolution records. Detailed chronological assessment of regional proxy records around the climatic transitions would allow better understanding of how regional records react to major global climatic transitions such as the Pleistocene-Holocene climatic transition.

To achieve this we extend our previous investigations on the Southeastern European loess belt (Constantin et al., 2019) to include other records from the region, as well as from the Chinese Loess Plateau and the central Great Plains, USA.

A less explored aspect in the study of loess-paleosol archives is the mechanism of soil formation and its development in eolian landscapes (Roberts, 2008). Conceptual models for the development of mineral magnetic records in soils and other pedogenic evidence of paleoenvironments under different regimes of eolian sedimentation can be discussed in terms of two end-members. These include extension of the pedogenetic processes downward into the parent loess material from a relatively stable land surface or top-down pedogenesis, and accretional or "up-building" soil formation in which the pedogenetic processes encompass the sediment as it accumulates over time (Almond and Tonkin, 1999; Kemp, 2001; Jacobs and Mason, 2007; Schaetzl and Anderson, 2009; Jordanova and Jordanova, 2020; Rousseau et al., 2021). These categories represent the extreme ends of a continuum; however, exclusive "top-down pedogenesis" is hardly realized in settings where dust was quasi-continuously deposited over hundreds of thousands of years, even during the Holocene (Albani et al., 2015; Longman et al., 2017; Lehmkuhl et al., 2021). The competition between loess sedimentation and soil formation processes is hard to test at mid-latitudes because the modern dust flux is low enough that it is integrated into surface soils without stratigraphic expression in the field. Muhs et al. (2004) documented the competing processes in an area of active loess deposition in southern Alaska. For determining the length of time over which loessic soils have developed Miao et al. (2015) present a model for a variety of conditions such as a cumulative (accretional) soil and a soil formed downward into the underlying loess.

The degree to which paleosols developed primarily through top-down or accretional pedogenesis is a crucial paleoclimate aspect of loess-paleosol research though often not discussed explicitly (Rousseau et al., 2017; Schaetzl et al., 2018). Where dust accumulation and loess formation is more or less continuous and accretional pedogenesis predominates, then at least some forms of pedogenetic alteration—soil structure formation, organic matter accumulation, and magnetic susceptibility enhancement, for example—can occur not long after the time of deposition. In this situation, a pedogenically overprinted sedimentary archive and the record of magnetic susceptibility or other paleoenvironmental proxies related to environmental changes and pedogenesis can be interpreted essentially as a time series, the usual interpretation in loess-paleosol studies (Zeeden et al., 2018). If dust accumulation is minimal for a significant period of time, then pedogenetic horizons form in previously accumulated sediment resulting in top-down pedogenesis that over time extends downward.

A straightforward argument in support of accretional pedogenesis at a given loess site is to show that continuous dust accumulation has occurred under a wide range of climatic conditions, from full-glacial to interglacial. Besides high-resolution dating constraints, pedostratigraphic evidence and stratigraphically consistent records of paleoenvironmental proxy parameters such as environmental magnetic susceptibility and grain size would allow assessment of the accretional character of the pedo-complex.

In the studied records, the Pleistocene-Holocene climatic transition is recorded by the broad transition from last glacial loess to the well-developed Holocene topsoil. Here we assess proxy variability in several loess-paleosol records from the Northern Hemisphere loess belt, covering the Pleistocene/Holocene climatic transition. We rely on luminescence dating of different grain-sizes of quartz separates for assessing regional response to the critical Pleistocene/ Holocene climate transition as recorded by loess deposits. We then compare our multi-site chronological data to test for synchronicity of response within deposits worldwide, and with other key global records of past climate variability. In interpreting each study site, we note evidence of all types in support of accretional pedogenesis.

2. Sites

This study gathers data from nine loess-paleosol sequences (LPS) across Europe, Asia, and North America (Fig. 1). These include the Baicaoyuan and Caoxian LPS in the Chinese Loess Plateau, Kuma in the loess-mantled Great Plains in Nebraska, and Smederevo in Serbia that are first discussed here. Other recently published records (Constantin et al., 2019; Groza-Sacaciu et al., 2020; Tecsa et al., 2020a) such as Roxolany and Kurortne from the loess belt north of the Black Sea, Ramnicu Sarat and Mircea Voda from the Lower Danube Basin loess, and Mošorin Veliki Surduk from the Middle Danube basin loess are also included in this overview. Details on luminescence sampling and stratigraphies are given in Figs. 2–10.

2.1. Sites from SE European loess belt

The Kurortne LPS (45°54′ N, 30°16′ E) is located near Kurortne village (Odessa region, Ukraine), at the Black Sea shore (Figs. 1, 2 and S2). The Roxolany LPS (46.2° N, 30.5° E) is located on the left bank of the Dniester estuary in southeastern Ukraine (Figs. 1, 3 and S3).

The Mircea Voda LPS (48.3° N, 28.2° E) is situated on the Dobrogea loess plateau, in the proximity of the Danube and the Black Sea (Figs. 1, 4, S1 and S4). The Ramnicu Sarat outcrop (45.5° N, 27.0° E; 160 m) is situated on the left bank of the Ramnicu Sarat river valley, at the northern edge of the Lower Danube Basin loess (Figs. 1, 5, S1 and S5).

The Mošorin Veliki Surduk LPS outcrops on the western slope of a 35 m deep gully, on the Titel Plateau, Vojvodina, Serbia (Figs. 1, 6, S1 and S6). The Smederevo site is an outcrop on the uppermost terrace on the Danube valley in the south of the extensively investigated loess plateaus in the Vojvodina region, Serbia (Figs. 1, 7, S1 and S7).

At these SE European Loess Belt LPS, the darkest and most prominent A horizon caps the top of a sedimentary section, with the appearance of a chernozem or similar soil typical of the steppe or forest steppe environments where these sites occur. Descriptions of the loess-soil profiles are provided in the Supplementary material.

2.2. Sites from the Chinese Loess Plateau

Caoxian LPS (36°22′29.40″ N, 104°37′18.19″ E, 2081 m a.s.l.) is located near the Caoxian village, Jingyuan County, Gansu Province, northwestern Loess Plateau (Fig. 1 and S8).The Caoxian section is situated on the sixth terrace of the Yellow River in Jingyuan Basin. At this section and others exposing the uppermost part of the loess-paleosol record on the Chinese Loess Plateau (CLP), there is an upward gradation from typical loess through lighter, less strongly expressed soil horizons to a dark, strongly expressed buried A horizon and then back to more weakly developed horizons again (Fig. 8 and S9).

Baicaoyuan LPS (36°15′50.80″ N, 105°08′05.21″ E, 2050 m a.s.l.) is located in Huining County, Gansu Province, in the northwest edge of the CLP (Fig. 1 and S8). In this section, there is an upward progression from typical loess through horizons displaying progressively greater pedogenic alteration, to a darker A horizon (Fig. 9 and S10).

2.3. Site from Great Plains loess, Nebraska, US

Kuma LPS (90.48064 N, 101.39258 W) is located in the western part of the Great Plains loess (Fig. 1, S1 and S12). Based on comparison with the nearby Wauneta (Miao et al., 2007) and Enders (Tecsa et al., 2020b) sections, the sequence here is correlated with the Pleistocene Peoria Loess (typical unweathered loess), the Pleistocene to Holocene Brady Soil (a sequence of transitional horizons grading up to a thick, dark A horizon), and the Holocene Bignell Loess (lighter-colored zone at the top of the section) (Fig. 10 and S12). The Brady Soil has previously been interpreted as an accretionary soil (Mason et al., 2008), in part because of the clear evidence for dust input under both glacial and interglacial climates in this region, including enhanced dust accumulation through much of the Holocene (Miao et al., 2007). The Bignell loess is much thicker at the Wauneta and Enders LPS because they are on the upwind edge of loess plateaus where coarse dust that became Bignell Loess was probably eroded proximally from older loess exposed on the plateau margin as well as from more distant sources. However, the field-observed morphology of the Brady Soil is very similar at those sites and at Kuma, and the stratigraphy of the Kuma site is more typical of large areas of the central Great Plains (Mason et al., 2003; Jacobs and Mason, 2007).

3. Methodology

3.1. Magnetic susceptibility sampling and measurements

Magnetic susceptibility samples were collected from the same profile as the luminescence samples and the continuous sampling resolution encompass 2 cm (for Kurortne, Roxolany, Mircea Voda) or 5 cm (for Mošorin Veliki Surduk, Smederevo, Baicaoyuan, Caoxian and Kuma) per sample, except for Ramnicu Sarat with samples collected 10 cm apart. For samples collected at Kurortne, Roxolany, Mošorin Veliki Surduk and Kuma, the volumetric magnetic susceptibility was measured at

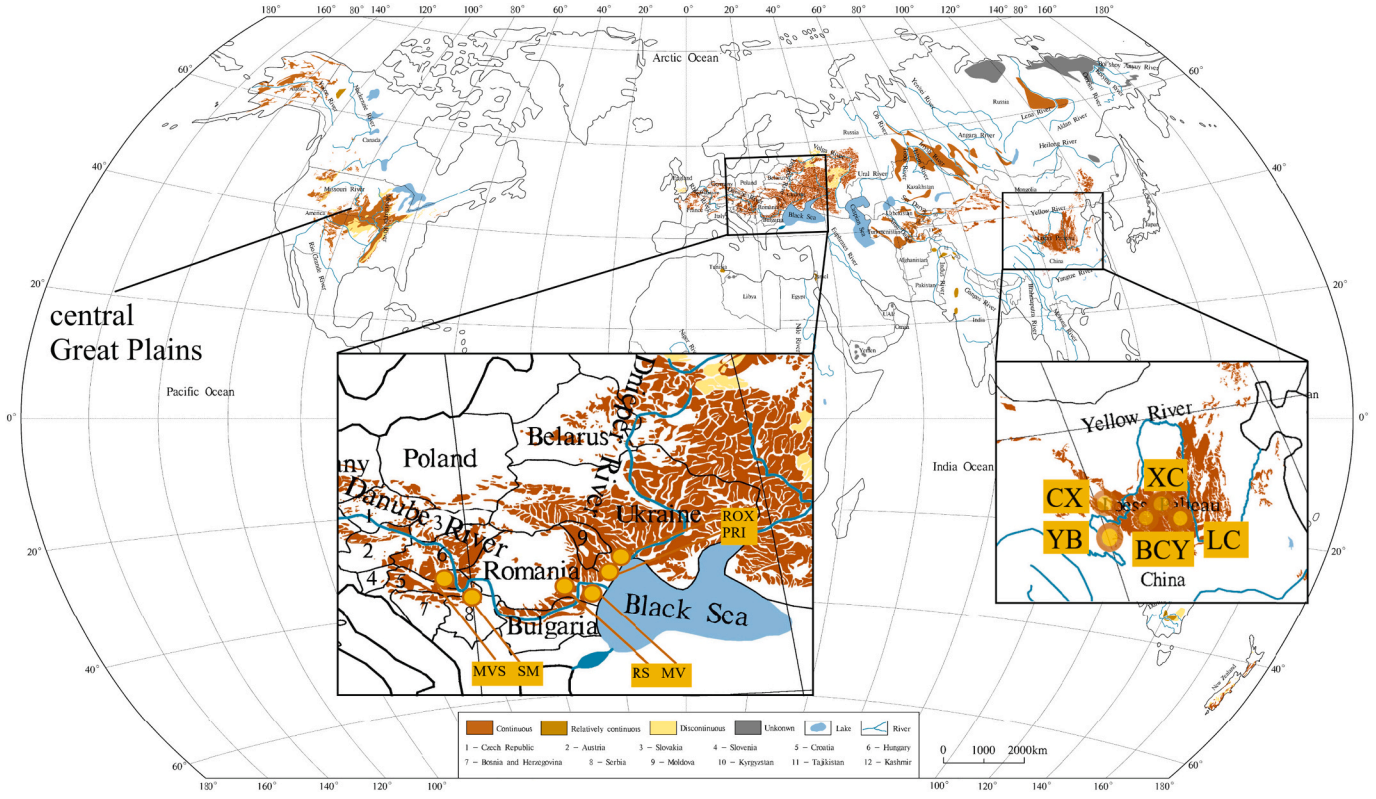

Fig. 1. Map of worldwide loess distribution modified after Li et al. (2020) provided by Yanrong Li. The investigated loess regions are indicated on the map. Right inset shows a close-up of the Chinese Loess Plateau and the investigated loess sites CX: Caoxian, BCY: Baicaoyuan, as well as other sites discussed in text, LC: Luochuan (Lu et al., 2013), XC Huanxian (Lu et al., 2006; Dong et al., 2015), YB Yuanbo (Lai and Wintle, 2006). Left inset gives a close-up of the central and southeastern European loess belt and shows the investigated study sites PRI: Kurortne (Tecsa et al., 2020a), ROX: Roxolany (Constantin et al., 2019), MV: Mircea Voda (Groza-Sacaciu et al., 2020), RS: Ramnicu Sarat (Constantin et al., 2019), SM: Smederevo, MVS: Mošorin Veliki Surduk (Constantin et al., 2019).

frequencies of 300 Hz and 3000 Hz in a static field of 300 mA/m using a Magnon International VSFM (sensitivity $\sim 10^{-7}$ SI) at University of Bayreuth, Germany. For samples from Mircea Voda, Ramnicu Sarat and Smederevo the magnetic susceptibility was measured at University of Bucharest, Romania with an AGICO MFK1-FA Kappabridge (sensitivity $\sim 2 \times 10^{-8}$ SI) using a magnetic field of 200 A/m and frequencies of 976 Hz and respectively 15,616 Hz. Samples collected from the CLP sites were measured using a Bartington MS2 Susceptibility Meter at Peking University, China.

All data were corrected for drift and for the effect of holder and sampling boxes (weak diamagnetism) and normalized to mass. Frequency dependence of magnetic susceptibility was expressed as a mass-specific loss of susceptibility $\chi_{fd} = \chi_{lf} - \chi_{hf}$, where χ_{lf} and χ_{hf} are the magnetic susceptibility measured at low and high frequency, respectively (Dearing et al., 1996). The frequency dependent magnetic susceptibility signals are attributed to the ultrafine-grained superparamagnetic minerals produced in situ as a result of pedogenic activity (e.g. Maher et al., 2003).

3.2. Luminescence dating

3.2.1. Sample collection and preparation

Luminescence samples were collected to closely bracket the transition between the loess unit and the Holocene soil, as identified visually in the field. The transition was tentatively identified as the visual boundary between proper loess and the overlying humus rich (A1 horizon) soil – the transitional zone would refer to the interval encompassing the genetic horizons (other than A1) that are clearly visible at all sites. Rather than denoting a sharp boundary, the loess-soil transition is marked in all sites by a transitional horizon encompassing clear litho/pedostratigraphic variability as seen in Figs. 2–10.

Luminescence samples were collected at high resolution, at intervals varying from 5 cm to 30 cm between samples, and for each LPS the number of samples judged necessary to include the full record of the Pleistocene-Holocene climatic transition, was determined based on litho- and pedostratigraphy. At some sites such as Caoxian and Kuma sites, more widely spaced samples, up to 1 m apart, were used to extend the chronology into underlying loess or overlying soil units. Sampling depths are given in Supplementary Tables S1–S9.

The material was collected by hammering stainless steel cylinders (6 cm in diameter and 20 cm in length) perpendicularly onto the freshly cleaned vertical profiles (Figs. S2–S7, S9–S10 and S12 – photos of the sampling profiles). The sealed tubes were opened under subdued red light at Babeș-Bolyai University luminescence laboratory, Cluj-Napoca, Romania. The material at both ends of the tubes was removed and used for gamma spectrometry measurements. From the remaining material in the inner part of the tubes quartz of different grain-sizes was extracted for luminescence measurements. In the first step, the bulk material was treated for several days with HCl (35% concentration) followed by H_2O_2 (30% concentration) in order to remove the carbonates and organic matter, respectively. The resulting material consisting of an undifferentiated polymineral mixture was wet sieved through a 63-μm mesh to separate between the fine and medium (<63 μm) and coarse fractions as they require different preparation procedures. The material with a diameter larger than 63 μm was further sieved to separate the 63–90 μm and 90–125 μm. It was enriched in quartz through a two-step density separation by centrifugation in a heavy liquid solution containing sodium metatungstate $Na_6[H_2W_{12}O_{40}]$ x H_2O. The lighter material (such as K-feldspars) was separated from quartz and plagioclase grains by centrifugation using 2.62 g/cm^3 density while heavy minerals such as zircons and apatite were isolated using 2.75 g/cm^3 density. The resulting mixture of quartz and plagioclase feldspars was treated with HF (40% concentration) for 40 min in order to dissolve the latter and to etch away the outer layer of quartz grains penetrated by alpha radiation. A rinse with HCl (10% concentration) for 60 min dissolved the fluorides precipitated during the HF treatment. The remaining quartz extracts were dry sieved to obtain the 63–90 μm and 90–125 μm fractions. For measurement, the coarse quartz grains were fixed in a monolayer on stainless steel disks (9 mm in diameter) using silicone spray.

The polymineral mixture material with a diameter smaller than 63

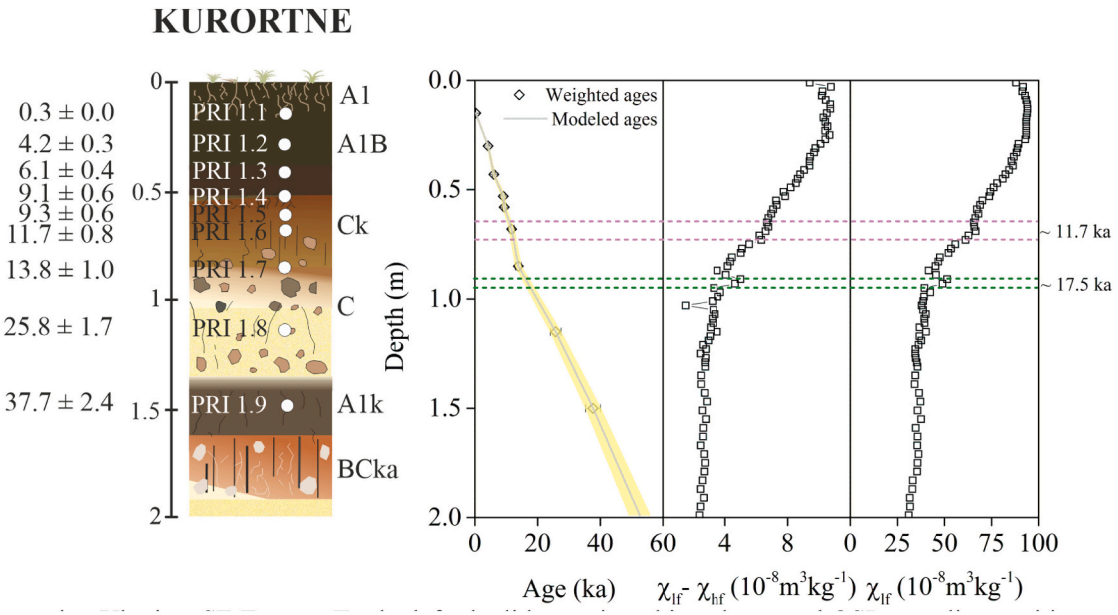

Fig. 2. Kurortne site, Ukraine, SE Europe. To the left, the lithostratigraphic column and OSL sampling positions and the weighted average OSL ages (ka) on 4–11 μm, 63–90 μm and 90–125 μm quartz. To the right, the weighted average luminescence ages and the modeled ages as function of depth. The uncertainty of the modeled ages represents the overall uncertainty calculated according to Aitken (1985). Also shown, the variation of the frequency dependent (χ_{lf}-χ_{hf}) and low frequency (χ_{lf}) magnetic susceptibility signals with depth. The dashed lines mark the depth interval dated to 17.5 ka and 11.7 ka within the error limits of the modeled ages. Soil horizons are labeled on the right side of the stratigraphic column. (A1) Soil – dark grey, (A1B) Soil – dark brownish-grey, (Ck) Soil to loess transition - pale yellowish-brown, (C) Loess – pale yellow, (A1k) Paleosol – brown, (BCka) Paleosol – light brown. (For interpretation of the references to colour in this figure legend, the reader is referred to the web version of this article.)

μm was processed to obtain the 4–11 μm quartz fraction by velocity settling in Atterberg cylinders using Stokes law followed by a 10 day digestion in H_2SiF_6 (concentration 35%) and density separation by centrifugation in distilled water. For measurement the aliquots were prepared by settling 2 mg of quartz on aluminium discs (9 mm in diameter).

3.2.2. Equivalent dose measurements

Equivalent dose measurements were carried out using TL/OSL Risø DA-20 readers (Bøtter-Jensen et al., 2010), equipped with classic or automated detection and stimulation head (DASH) (Lapp et al., 2015). The luminescence signals were detected through 7.5 mm thick Hoya U-340 filters placed in front of EMI 9235QA or PDM 9107Q-AP-TTL-03 photomultipliers, depending on the reader type. Irradiations were performed using build-in $^{90}Sr/^{90}Y$ (beta irradiation) sources calibrated using calibration quartz provided by the Nordic Laboratory for Luminescence Dating.

The equivalent doses were measured using the Single Aliquot Regenerative dose (SAR) protocol (Murray and Wintle, 2000, 2003). The quartz luminescence emission was stimulated with blue light emitting diodes for 40 s at 125 °C and the net CW-OSL signal was isolated from the first 0.304 s of luminescence emission minus a background assessed from the 1.69–2.03 s of luminescence emission. The OSL response to a test dose of 17 Gy was used to correct for sensitivity changes in all investigations presented in this study, except for the case of equivalent dose determination of very young samples (De < 5 Gy), when a test dose of 4 Gy was employed. A preheat temperature of 220 °C for 10 s and a cutheat of 180 °C were employed. At the end of each SAR cycle a high-temperature bleach for 40 s at 280 °C was performed by stimulation with blue diodes (Murray and Wintle, 2003). Any possible quartz contamination with feldspars was monitored through exposure to IR diodes in the IR depletion test (Duller, 2003) employed on each aliquot measured. The performance of the SAR protocol was evaluated using the standard intrinsic tests (Recycling and Recuperation ratios). The acceptance criteria were 10% deviation from unity for the Recycling and IR depletion ratios and a maximum of 3% of the natural signal for the Recuperation ratio. We have used similar measurement conditions for all luminescence samples investigated in this study.

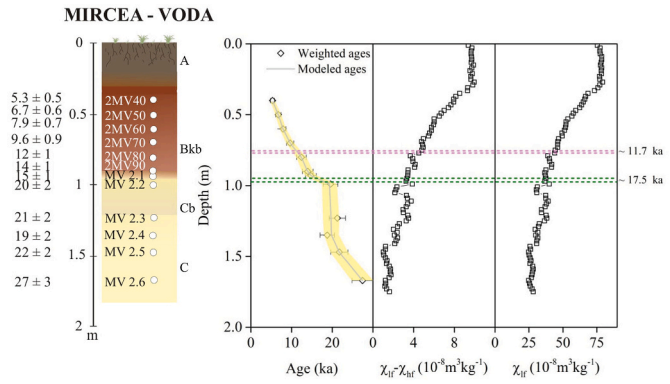

Fig. 4. Mircea-Voda site, Romania, SE Europe. To the left, the lithostratigraphic column, OSL sampling positions and the weighted average OSL ages (ka) on 4–11 μm and 63–90 μm quartz. To the right, the weighted average luminescence ages and the modeled ages as function of depth. The uncertainty of the modeled ages represents the overall uncertainty calculated according to Aitken (1985). Also shown, the variation of the frequency dependent (χ_{lf}-χ_{hf}) and low frequency (χ_{lf}) magnetic susceptibility signals with depth. The dashed lines mark the depth interval dated to 17.5 ka and 11.7 ka within the error limits of the modeled ages. Soil horizons are labeled on the right side of the stratigraphic column. (A) Soil – brown, (Bkb) Soil – brownish, (Cb) Loess-very pale yellow, (C) Loess – pale yellow. (For interpretation of the references to colour in this figure legend, the reader is referred to the web version of this article.)

3.2.3. Annual dose measurements

For annual dose measurements, the material was dried and finely ground before being sealed in the gamma spectrometry measurement tubes and left for one month to allow ^{222}Rn achieve secular equilibrium with the ^{238}U series. Radionuclide activity concentrations were

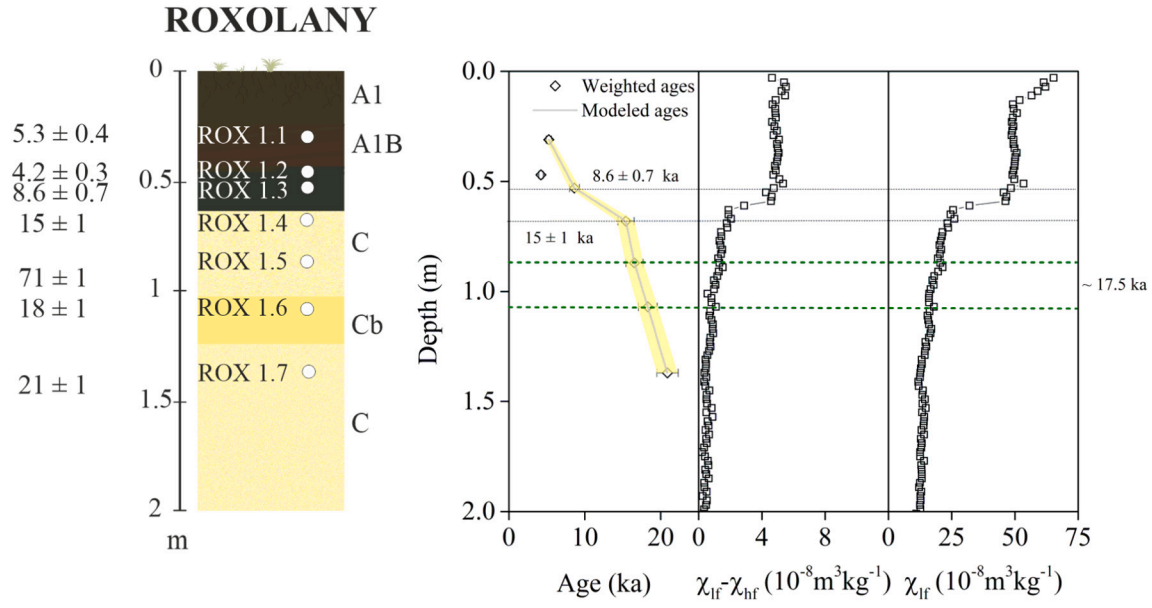

Fig. 3. Roxolany site, Ukraine, SE Europe. To the left, the lithostratigraphic column and OSL sampling positions and the weighted average OSL ages (ka) on 4–11 μm, 63–90 μm and 90–125 μm quartz. To the right, the weighted average luminescence ages and the modeled ages as function of depth. The uncertainty of the modeled ages represents the overall uncertainty calculated according to Aitken (1985). Also shown, the variation of the frequency dependent (χ_{lf}-χ_{hf}) and low frequency (χ_{lf}) magnetic susceptibility signals with depth. The dotted lines mark the depth interval where a hiatus in OSL ages occurs. The short dashed lines indicate the depth interval dated to 17.5 ka within the error limits of the modeled ages. Soil horizons are labeled on the right side of the stratigraphic column. (A1) Soil – dark grey to black, (A1B) Soil – brownish to grey, (Cb) Incipient soil, yellowish brown, (C) Loess – pale yellow. (For interpretation of the references to colour in this figure legend, the reader is referred to the web version of this article.)

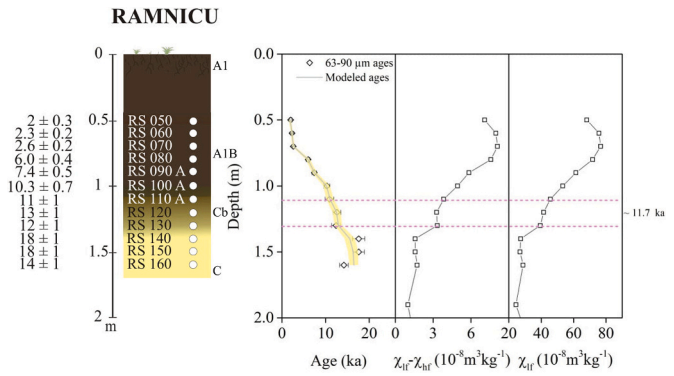

Fig. 5. Ramnicu Sarat site, Romania, SE Europe. To the left, the lithostratigraphic column, OSL sampling positions and the 63–90 μm quartz OSL ages (ka). To the right, the luminescence ages and the modeled ages as function of depth. The uncertainty of the modeled ages represents the overall uncertainty calculated according to Aitken (1985). Also shown, the variation of the frequency dependent (χ_{lf}-χ_{hf}) and low frequency (χ_{lf}) magnetic susceptibility signals with depth. The dashed lines mark the depth interval dated to 11.7 ka within the error limits of the modeled ages. Soil horizons are labeled on the right side of the stratigraphic column. (A1) Soil – brown, (A1B) Soil – brownish to grey, (Cb) Loess-very pale yellow, (C) Loess – pale yellow. (For interpretation of the references to colour in this figure legend, the reader is referred to the web version of this article.)

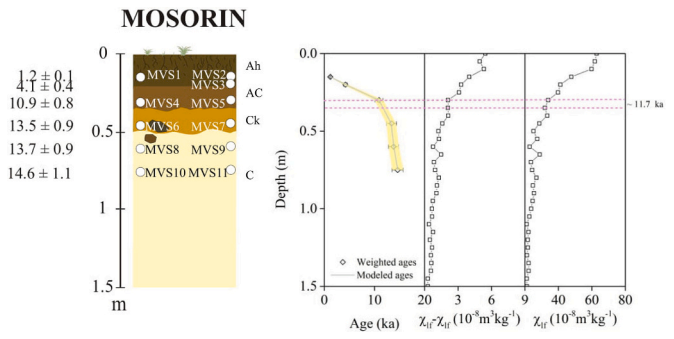

Fig. 6. Mošorin Veliki Surduk site, Serbia, SE Europe. To the left, the lithostratigraphic column, OSL sampling positions and the weighted average OSL ages (ka) on 4–11 μm and 63–90 μm quartz. To the right, the weighted average luminescence ages and the modeled ages as function of depth. The uncertainty of the modeled ages represents the overall uncertainty calculated according to Aitken (1985). Also shown, the variation of the frequency dependent (χ_{lf}-χ_{hf}) and low frequency (χ_{lf}) magnetic susceptibility signals with depth. The dashed lines mark the depth interval dated to 11.7 ka within the error limits of the modeled ages. Soil horizons are labeled on the right side of the stratigraphic column. (Ah) Soil – brown greyish, (AC) Soil – reddish brown, (Ck) Soil to loess transition - pale yellowish brown, (C) Loess - pale yellow. (For interpretation of the references to colour in this figure legend, the reader is referred to the web version of this article.)

determined based on high resolution gamma spectrometry using a hyper-pure germanium well detector. The conversion factors reported by Guérin et al. (2011) were used to derive the annual dose rates. The total dose rate consists of the contribution from the beta and gamma radiations for coarse grains as well as the contribution from alpha radiations in the case of fine grains. Adopted alpha efficiency factor was 0.04 ± 0.02 (Rees-Jones, 1995) to correct for the lower efficiency of alpha radiation in inducing luminescence for 4–11 μm quartz. Beta attenuation and etching factors used for 63–90 μm and 90–125 μm quartz were 0.94 ± 0.05 and 0.92 ± 0.05, respectively (Mejdahl, 1979). An internal dose rate of 0.010 ± 0.002 Gy/ka was considered (Vandenberghe et al., 2008). The contribution of cosmic radiation was estimated following the equation published by Prescott and Hutton (1994).

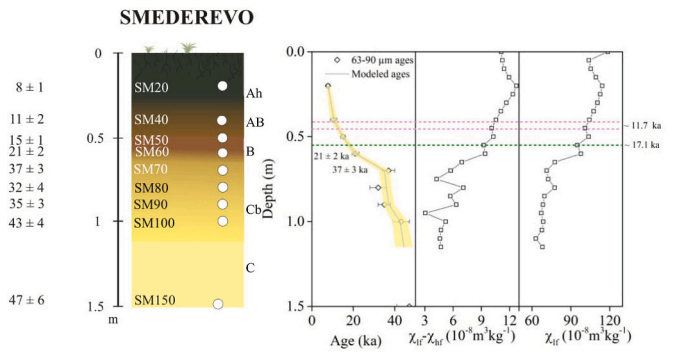

Fig. 7. Smederevo site, Serbia, SE Europe. To the left, the lithostratigraphic column, OSL sampling positions and the 63–90 μm quartz OSL ages (ka). To the right, the luminescence ages and the modeled ages as function of depth. The uncertainty of the modeled ages represents the overall uncertainty calculated according to Aitken (1985). Also shown, the variation of the frequency dependent (χ_{lf}-χ_{hf}) and low frequency (χ_{lf}) magnetic susceptibility signals with depth. The dashed lines mark the depth interval dated to 17.5 ka and 11.7 ka within the error limits of the modeled ages. Soil horizons are labeled on the right side of the stratigraphic column. (Ah) Soil – brown greyish, (AB) Soil – brown, (B) Soil - reddish brown, (Cb) Loess- very pale yellow, (C) Loess-pale yellow. (For interpretation of the references to colour in this figure legend, the reader is referred to the web version of this article.)

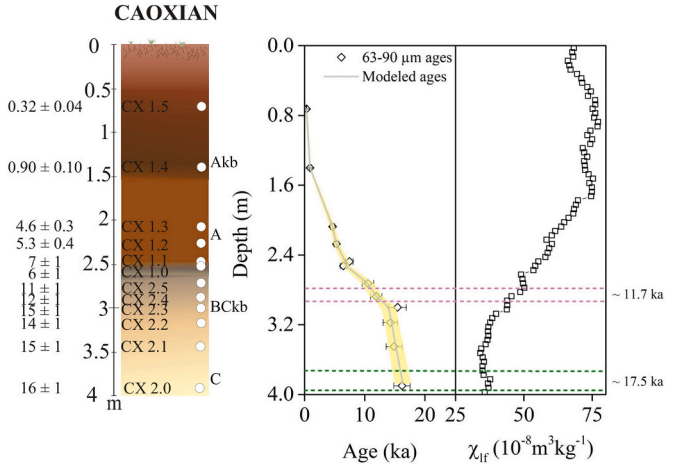

Fig. 8. Caoxian site, Chinese Loess Plateau. To the left, the lithostratigraphic column, OSL sampling positions and the 63–90 μm quartz OSL ages (ka). To the right, the luminescence ages and the modeled ages as function of depth. The uncertainty of the modeled ages represents the overall uncertainty calculated according to Aitken (1985). Also shown, the variation of low frequency (χ_{lf}) magnetic susceptibility signals with depth. The dashed lines mark the depth interval dated to 17.5 ka and 11.7 ka within the error limits of the modeled ages. Soil horizons are labeled on the right side of the stratigraphic column. (Akb) Soil – dark brown, (A) Soil – dark brown reddish, (BCkb) Transition from soil to loess – grey yellowish, (C) Loess – pale yellow. (For interpretation of the references to colour in this figure legend, the reader is referred to the web version of this article.)

To correct for the attenuation effect on the absorbed dose by the quartz grains, induced by the water surrounding the minerals in the loess matrix, estimation of the average water content during burial is required. For this we took into consideration the difference between the “in situ” and the oven dried weight of material with a relative error of 25% as well as information on past humidity variation in other sites in the investigated regions. The values for radionuclide concentrations as well as the total dose rates for all samples discussed in this paper are found in Tables S1–S9.

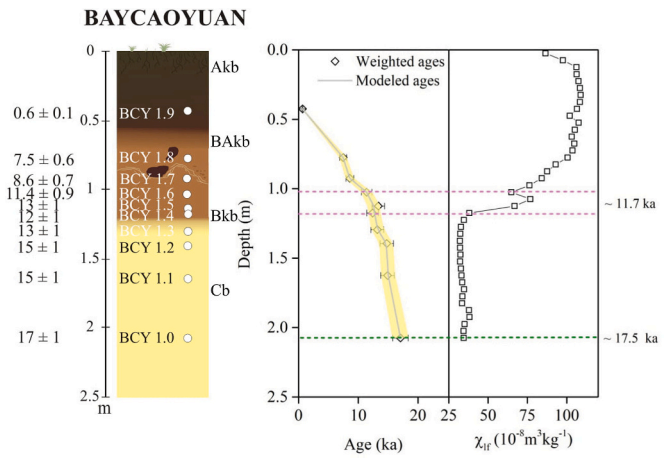

Fig. 9. Baicaoyuan site, Chinese Loess Plateau. To the left, the lithostratigraphic column, OSL sampling positions and the weighted average OSL ages (ka) on 4–11 μm and 63–90 μm quartz. To the right, the weighted average luminescence ages and the modeled ages as function of depth. The uncertainty of the modeled ages represents the overall uncertainty calculated according to Aitken (1985). Also shown, the variation of the low frequency (χ_{lf}) magnetic susceptibility signals with depth. The dashed lines mark the depth interval dated to 17.5 ka and 11.7 ka within the error limits of the modeled ages. Soil horizons are labeled on the right side of the stratigraphic column. (Akb) Soil – dark brown, (BAkb) Soil – pale brown, (Bkb) Transition from soil to loess – very pale brown, (Cb) Loess – very pale yellow. (For interpretation of the references to colour in this figure legend, the reader is referred to the web version of this article.)

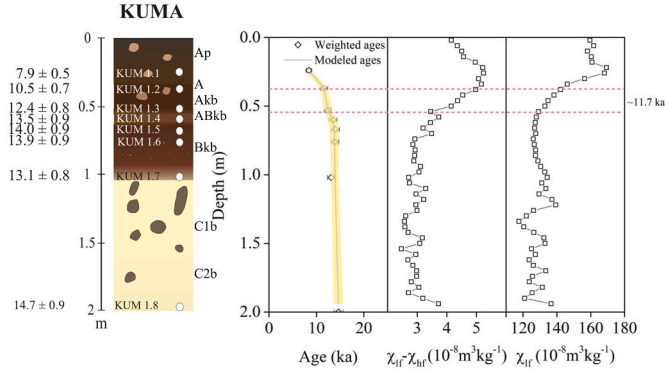

Fig. 10. Kuma site, Nebraska, US. To the left, the lithostratigraphic column and OSL sampling positions and the weighted average OSL ages (ka) on 4–11 μm, 63–90 μm and 90–125 μm quartz. To the right, the weighted average luminescence ages and the modeled ages as function of depth. The uncertainty of the modeled ages represents the overall uncertainty calculated according to Aitken (1985). Also shown, the variation of the frequency dependent (χ_{lf}-χ_{hf}) and low frequency (χ_{lf}) magnetic susceptibility signals with depth. The dashed lines mark the depth interval dated to 11.7 ka within the error limits of the modeled ages. Soil horizons are labeled on the right side of the stratigraphic column. (Ap) Soil – dark brown, (A) Soil – dark brown reddish, (Akb) Soil – dark brown, (ABkb) Soil-brown greyish, (Bkb) Transition from soil to loess – very pale brown, (C1b) Loess – very pale yellow. (C2b) Loess – very pale yellow greyish. (For interpretation of the references to colour in this figure legend, the reader is referred to the web version of this article.)

3.3. Modeling of luminescence ages and accumulation rates

For generating age-depth models, we used the ADMin software (Zeeden et al., 2018). This age-depth Bayesian modeling approach makes no assumptions on accumulation rates, but assumes luminescence ages and their uncertainties to be correct. Initially, the method separates the overall uncertainty into a random and systematic part; here a separation based on luminescence uncertainties (Tables S1–S9) is used.

For the samples where one set of ages on different quartz grain-size fractions was reported, we calculated the overall uncertainty by combining in quadrature the random and systematic components (Aitken, 1985, Appendix B). On multiple grain-sizes of quartz, we determined the overall random and overall systematic uncertainty as well as the overall uncertainty on the weighted average age according to Aitken (1985, Appendix B). For deriving accumulation rates, we used the random uncertainty only. In addition, we used the computer code from Zeeden et al. (2018), but adjusted it to also output the individual Monte Carlo sampling chains. From these, the accumulation rate and related uncertainty was determined. This allows for somewhat more confined accumulation rate models, compared to using only the uncertainty of (modeled) ages.

4. Results

4.1. Luminescence characteristics and equivalent doses

All quartz samples investigated emitted a luminescence signal during exposure to blue LEDs for 40 s at 125 °C, which decayed rapidly with stimulation time. Representative luminescence decay curves of each grain-size fraction investigated are compared with those on calibration quartz supplied by the Nordic Luminescence Laboratory (Fig. S13 insets). It can be seen that their shapes are indistinguishable thus indicating that the sampled luminescence emission used for equivalent dose determination is dominated by the fast luminescence component. This is the luminescence emission that bleaches first and very rapidly upon light exposure. This increases the likelihood that no significant residual signal from previous erosion and transportation cycles affects the measured luminescence signal, a prerequisite for applying the SAR protocol (Murray and Wintle, 2000).

The equivalent doses were determined by interpolating the sensitivity corrected natural OSL signal onto the laboratory dose-response curve constructed for each aliquot. Representative SAR luminescence dose-response curves are illustrated in Fig. S13 for individual aliquots of fine (4–11 μm) and coarse (63–90 μm and 90–125 μm) grained quartz from Baicaoyuan, Caoxian and Kuma samples. The intrinsic tests of the SAR protocol have been successfully passed as it is demonstrated by the overlap of Recycling and IR depletion points and their corresponding regeneration points and by the fact that the laboratory dose response curve passes close to the origin of the axes.

We have investigated the influence of the temperature of the preheat, carried out prior to the OSL signal read-out, on the measured equivalent dose using samples from Roxolany, Ramnicu Sarat, Mošorin, Baicaoyuan and Kuma. As seen in Fig. S14 the equivalent doses are similar for preheat temperatures ranging from 200 to 240 °C.

We used the combination of preheat for 10 s at 220 °C with cutheat to 180 °C for the dose recovery test and the given irradiation dose approximated the equivalent dose, as in the investigations on previously published sites. The SAR protocol accurately measured known irradiation doses given prior to any heating treatments (Fig. S15). Thus, the combination of preheat for 10 s at 220 °C with cutheat to 180 °C used to measure all equivalent doses, except for the samples in Mošorin Veliki Surduk, where slightly lower temperatures were used (Constantin et al., 2019). The equivalent doses and the number of aliquots used for averaging are given in Tables S1–S9 for all the investigated sites.

Because we have dated samples collected from soil or from the loess-soil transition using luminescence method we investigate the degree to which post-depositional processes such as grain mixing due to bioturbation might affect the accuracy of the measured equivalent doses and consequently that of the ages. A test for bioturbation or other mixing processes using luminescence measurements can be made by investigating the degree of spread in equivalent doses data beyond that expected based on individual equivalent dose uncertainties (i.e., overdispersion) (Bateman et al., 2007; Galbraith and Roberts, 2012;

Gliganic et al., 2015; Hanson et al., 2015; Constantin et al., 2019).

We have quantified the spread in the equivalent doses on the Baicaoyuan sample BCY 1.2, collected from the transition from last glacial loess to Holocene soil (Fig. S16), by measuring 51 aliquots of the 63–90 μm quartz separate and by determining the overdispersion calculated from the Central Age Model (Galbraith et al., 1999). As seen in the radial plot in Fig. S16, 71% of the measured equivalent doses agree within 2-sigma uncertainty with the mean equivalent dose. The overdispersion calculated from the Central Age Model (Galbraith et al., 1999) is 14%. We interpret these values as normal, as natural samples of quartz rarely yield equivalent dose estimates that are statistically concordant with respect to their within-aliquot standard errors (Galbraith and Roberts, 2012). Even in the absence of complicating factors such as post-depositional mixing there is commonly 10–20% overdispersion among equivalent dose estimates from single aliquots (Galbraith and Roberts, 2012; Constantin et al., 2019).

We also constructed radial plots for 63–90 μm and 90–125 quartz equivalent doses measured on soil and loess samples from Kurortne and Kuma LPS (Fig. S16). For Kurortne 33%, 25% and 25% of the individual equivalent doses agree within 2-sigma uncertainty to the mean equivalent doses obtained on soil sample PRI 1.2, transitional horizon sample PRI 1.6 and loess sample PRI 1.8, respectively. The overdispersions calculated for these samples are 25%, 23% and 22% respectively (Table 1). The mean equivalent doses incorporate within 2-sigma uncertainty 55% of individual equivalent doses for the soil sample KUM 1.4 and 42% for sample KUM 1.7 collected from the transition from loess to the Holocene soil. The overdispersions calculated for these two samples are 6% and 9% respectively.

In Table 1 we present scatter data expressed as relative standard error, RSD (%), and overdispersion, OD (%), in multigrain aliquots of 63–90 μm quartz extracted from both soil and loess samples from the Kurortne, Mircea Voda, Caoxian, Baicaoyuan and Kuma. Together with the previously published data on the Roxolany, Ramnicu Sarat and Mošorin (see Fig. S7 in Constantin et al. (2019)) we observe that the RSD and OD values are generally below 20% for soil and loess samples from Chinese Loess Plateau and Great Plains sites. The SE European sites generally yield overdispersion values around 25%, with a few up to 30% in some uppermost soil samples, some of which may be explainable by modern agricultural disturbance.

This analysis of luminescence data gives us confidence that post-depositional mixing does not significantly affect our chronological results on the timing of the Pleistocene-Holocene climatic transition as inferred from magnetic susceptibility profiles, since at that depth there is little evidence of greater mixing than in the underlying loess, based on the luminescence data (Table 1). The luminescence data also indicate little difference in the extent of post-depositional mixing between soils and underlying loess at the Chinese Loess Plateau and Great Plains sites, supporting interpretation of the soil ages as primarily recording time of dust deposition, though the latter point is more ambiguous for the SE European LPS.

4.2. OSL ages

Luminescence dating for this study was performed using up to three grain-size classes (4–11 μm, 63–90 μm, 90–125 μm) of quartz extracted from the same sample. Such an approach is rare and time-consuming but can reduce the random uncertainty of the age of a sample. Quartz grains in multiple size fractions can be considered independent dosimeters, yielding multiple ages for the same sample. This is due to the difference in the targeted grain diameter which, in turn influences the degree of attenuation and absorption of alpha, beta and gamma radiation that form the natural radioactive field surrounding the grain. The small diameter of fine grains of quartz (4–11 μm) allows alpha radiation to pass through the entire grain while the coarser material (> 63 μm) fully attenuates the alpha irradiation within the outer layer of the grain which is then etched away in the sampling preparation stage. In addition, the natural reduction in size of the fine quartz grains likely occurred over many cycles of erosion, transport and deposition and consequently irradiation and bleaching cycles that sensitize the grains.

With that background, by taking the weighted average of the luminescence dates obtained from multiple grain-size fractions of a single sample, which are assumed to be coeval, the overall random uncertainty can be reduced (Aitken, 1985, Appendix B). The contribution of the random sources of uncertainty to the individual luminescence ages is a measure of their precision. Thus by using weighted average ages from a suite of quartz grain sizes we aim at obtaining a more precise age of the dated sedimentary context.

Figs. 2–10 show the luminescence chronologies as well as the modeled ages obtained for all the sites investigated. Individual luminescence ages on each grain-size fraction of quartz and the weighted average age calculated following Aitken (1985) Appendix B are presented in Tables S1–S9. Uncertainties on the individual ages were calculated based on the error assessment system described by Aitken and Alldred (1972) and Aitken (1976).

The systematic uncertainties on the individual ages for the fine grains amount to 8–10% while for coarse grains vary from 6% to 8%. The main sources of systematic errors are the estimates of the uncertainties associated with the time-averaged water content, alpha efficiency, and beta attenuation factors (Aitken, 1985).

The random uncertainty represents a measure of the internal consistency of the optical ages. For coarse grains, they extended to 9% except for some uppermost soil samples where the contribution increases up to 13–33%. In the case of the fine grains, the random error varies up to 6–8%.

Following Aitken (1985, Appendix B) we calculated weighted averages on fine and coarse quartz ages (see Tables S1–S3, S5, S8–S10). The total uncertainty associated with the weighted average age was calculated by first quantifying the random and the systematic components and by propagating them in quadrature.

In this way, the contribution of the random uncertainty to the overall uncertainty in the weighted average age was reduced to 2–3% except in the case of four samples where the contribution ranged from 4 to 7%. We obtained an overall uncertainty in the weighted average ages ranging from 6 to 9%. To conclude, by weighting the fine and coarse quartz ages resulted in a decrease of 2% up to 6% in the total uncertainty of the age estimates.

5. Dating of magnetic susceptibility enhancement using optically stimulated luminescence

The loess-paleosol environmental magnetic signal can be separated in two components: the lithogenic component, dependent on the properties of the deposited dust (e.g., provenance, grain-size), which is responsible for most of magnetic signal in loess layers, and the pedogenic component, dependent mostly on soil forming factors (including climate, vegetation, drainage, soil development time), which is responsible for most of the magnetic signal acquired in paleosols. Due to the fact that dust deposition continued as paleosols developed, the pedogenetically enhanced component can also be separated into a syndepositional signal acquired during deposition of a particular interval within the sequence, and a post-depositional enhancement acquired while that interval remains shallow enough to the ground surface to be affected by pedogenesis (Miao et al., 2006 and references therein). Syndepositional pedogenesis is overprinted by post-depositional alteration, both for accretional soils and for soils that form downward from a stable land surface; this occurs over a depth ranging from tens of centimeters to several meters, depending on the regional climate and other factors. Recent work by Jordanova and Jordanova (2020, 2021) provides a comprehensive new analysis of these issues.

The magnetic properties of loess-paleosols such as mass specific low-field magnetic susceptibility (χ_{lf}) and its dependence on the frequency of the applied field (χ_{fd}) are widely used for disentangling the intensity of

Table 1
Relative standard deviation, RSD, (%) and equivalent dose overdispersion, OD, (%) calculated for 63–90 μm and 90–125 μm quartz extracted soil and loess samples from the following sites: Kurortne (Ukraine), Mircea Voda (Romania), Caoxian and Baicaoyuan (China) and Kuma (Nebraska).

Unit	Profile name	Sample code	Grain-size (μm)	De ± st. err.	Number of aliquots	RSD (%)	OD (%)
Holocene soil	Kurortne	PRI 1.2	63–90	15 ± 1	10	29	26
			90–125	14 ± 1	12	27	25
Loess-soil transition		PRI 1.6	63–90	38 ± 2	10	13	12
			90–125	35 ± 3	12	26	23
Loess		PRI 1.8	63–90	89 ± 4	10	14	13
			90–125	63 ± 4	12	22	22
Holocene soil	Mircea Voda	2MV60	63–90	22 ± 2	21	32	30
		2MV80	63–90	36 ± 3	18	31	31
Loess-soil transition		2MV2.2	63–90	54 ± 3	23	21	21
Loess		2MV2.6	63–90	87 ± 4	20	23	22
Holocene soil	Caoxian	CX1.3	63–90	13.4 ± 0.3	13	9	6
Loess-soil transition		CX2.5	63–90	30 ± 2	15	23	14
Loess		CX2.2	63–90	41 ± 2	14	16	15
Holocene soil	Baicaoyuan	BCY 1.8	63–90	23 ± 1	10	12	12
Loess-soil transition		BCY 1.3	63–90	39 ± 1	13	13	12
		BCY 1.2	63–90	42 ± 1	51	14	14
Loess		BCY 1.0	63–90	48 ± 2	11	11	9
Holocene soil	Kuma	KUM 1.4	63–90	52 ± 1	22	7	6
Loess-soil transition		KUM 1.7	63–90	54 ± 1	19	10	9

soil forming processes, as well as the chemical weathering of primary loess. The χ_{fd} is a highly diagnostic proxy for the exclusively pedogenetically formed fraction of ferrimagnetic minerals (Maher et al., 2003).

The pedogenic enhancement of the magnetic susceptibility is controlled in a complex way by climate through precipitation, temperature, and evapotranspiration rate, reflecting long-term shifts and variability in soil humidity (e.g. Maher and Thompson, 1994, 1995; Orgeira and Compagnucci, 2006; Orgeira et al., 2011; Song et al., 2014; Hu et al., 2015). The latter is controlled by wind, temperature, vegetation and local conditions. As such, the trends in χ_{lf} and χ_{fd} are often regarded as reliable paleoclimate proxies for inferring local hydroclimate variability (e.g. Maher and Thompson, 1994, 1995; Schaetzl et al., 2018).

An alternative method to distinguish between interglacial deposits and pedogenically-overprinted glacial loess is based on the concentration variations of coarse-grained eolian (magnetically pseudo-single domain and multidomain) magnetite (Liu et al., 2004). It is based on the differences in low temperature properties between the coarse-grained (multidomain and pseudo-single domain) detrital magnetite and the pedogenic magnetic particles including superparamagnetic (SP) particles and relatively larger (>SP) maghemite particles, the eolian coarse-grained magnetite, the latter being very sensitive to the changes in the intensity of the winter monsoon, and in turn related to the changes in paleoclimate. However, Liu et al. (2004) point out that more studies are necessary on recent soil to further check the validity of the new method.

A gradual increase in magnetic susceptibility values, along with other evidence of synsedimentary pedogenesis, marks the transition from the Last Glacial loess to the Holocene soil in most of the loess-paleosol sections from the Danube Basin and Black Sea coast in Eastern Europe (e.g. Marković et al., 2015; Necula et al., 2015; Jordanova and Jordanova, 2020), Chinese Loess Plateau (e.g. Maher et al., 2003; Dong et al., 2015) and Great Plains (Nebraska, United States) (e.g. Tecsa et al., 2020b).

Since in loess studies there is no established approach of constraining the interval in the magnetic susceptibility record that reflects the Pleistocene-Holocene boundary we adopted an approach similar to Stern and Lisiecki (2014). We observe the variation of the χ_{fd} values over the transition from the Last Glacial maximum (LGM) to Holocene through two temporal reference points: 17.5 ka and 11.7 ka.

For each studied LPS we determine the depth where the χ_{fd} values increase significantly and continuously (Figs. 2–10) compared to those values that characterize the late glacial loess (or where available LGM loess). On samples around the selected depth, an independent two-sample unpaired *t*-test was conducted in order to quantify the difference between the mean values of χ_{fd} (χ_{lf} for Caoxian and Baicaoyuan) in loess and from the transition from loess to soil. For all sites, at the 0.05 level, the difference of the population means is significantly less than the assumed hypothesis ($t = 0$, the two means are similar) (Table S10). This implies that the χ_{fd} values for the transition from loess to soil are significantly higher than the χ_{fd} values for loess.

From the age model obtained for each LPS we estimate the age corresponding to the depth where the χ_{fd} values increase significantly and continuously and interpret that age as the onset of the Pleistocene-Holocene climatic transition. This approach assumes at least some degree of accretionary pedogenesis, so that at the depth of initial magnetic susceptibility increase, magnetic enhancement was primarily acquired soon after the loess at this depth accumulated, when it was much closer to the land surface. In the Discussion, we expand on the issues involved in confirming the occurrence of accretional pedogenesis at the studied LPS and its implications for formation of the soils and magnetic susceptibility records, explaining why we conclude that there is clear evidence for accretional pedogenesis at the Chinese Loess Plateau and Great Plains LPS and it also had a substantial role at the SE European LPS.

We also consider how the timing of the climatic transition compares to the date of 11.7 ka for the Pleistocene-Holocene boundary as defined in ice-core records (Rasmussen et al., 2014; Walker et al., 2019) and the age of 17.5 ka for Termination 1 identified in benthic $\delta^{18}O$ records in North Atlantic (Stern and Lisiecki, 2014).

5.1. SE European Loess Belt sites

At Kurortne (KR), located on the northern sea-shore of the Black Sea in Ukraine, from the base of the sequence the χ_{fd} increases very slowly up to ~17 ka and accelerates in two steps after 17.5 ka and around 11.7 ka until it reaches a constant level after 4 ka (Fig. 2). The onset of enhancement in magnetic susceptibility is thus identified prior to the loess-soil transition identified visually in the field that was dated around 11.7 ka. At Roxolany (ROX) on the Dniester estuary in Ukraine, the χ_{fd} values start to increase slowly before 17.5 ka (~1.29 m) until around 15 ka at 0.68 m depth (Fig. 3). A very sharp increase in χ_{fd} values occurs between 0.63 m and 0.55 m but an age gap of ~5 ka is indicated by OSL ages over this depth interval as well as by the sharp and undulating boundary. For the soil horizons younger than 8.6 ± 0.7 ka, the χ_{fd} values remain stable. The onset of increase in χ_{fd} values (~20 ka) precedes the loess-soil transition identified in the field here as well (Fig. S3).

One explanation for the sharp transition of χ_{fd} and age gap can be the effect of top-down soil development at a time of minimal dust

accumulation (Roberts, 2008), with substantial mixing in soil above the age gap and downward extension of a weathering front producing the sharp increase in magnetic susceptibility. However, intense mixing is not supported by the luminescence data from this site (Constantin et al., 2019). Also, the intensity of both χ_{lf} and χ_{fd} signals in Roxolany samples are lower than all other European sites investigated here as well as reported in the literature (Marković et al., 2015; Panaiotu et al., 2001), inconsistent with a period of substantial top-down pedogenesis. The age gap suggests instead an erosional event and a gap in the record corresponding to the sharp χ_{fd} increase. Accumulation rates for the Holocene soil horizons younger than 8.6 ± 0.7 ka add support to this interpretation. (see Section 6).

At the Mircea Voda site (MV), Lower Danube basin, starting from the base of the sampled loess unit dated around 20 ka, the χ_{fd} values display a tendency to increase slowly up to 11.7 ka after which the increase is more accelerated (Fig. 4). The χ_{fd} values remain constant after 5 ka for the uppermost 0.35 cm of the profile. It is worth noting that in Mircea Voda, the onset of increase in χ_{fd} values also occurs prior to the loess-soil transition identified in the field which is dated around 17.5 ka. A smooth increase in χ_{fd} values is seen along the loess-soil transition at Ramnicu Sarat (RS) from the northern edge of the Lower Danube Basin (Fig. 5). Due to strong scatter in OSL ages dated to before 12 ka we can only conclude that the χ_{fd} values are already significantly high around 12 ka. Also at this depth (130 cm) the transition between loess and soil horizon was visually identified (Fig. 5 and S5).

At the Mošorin Veliki Surduk site (MVS), Middle Lower Danube basin, the χ_{fd} values increase slowly and smoothly up to 14 ka (Fig. 6). The rate of growth accelerates around 11.7 ka and continues to increase until around 1.2 ka. The transition from loess to soil identified visually in the field is dated around 14 ka (Fig. S6). Smederevo site, along the Danube River in Serbia, displays a rapid increase in χ_{fd} values much earlier than in all other sites, before 21 ka, that continues at a relatively steady rate until 7.8 ± 0.8 ka, after which a decreasing trend is observed (Fig. 7). Please note an age difference of ~15 ka between 0.7 and 0.6 m (37 ± 3 ka and 21 ± 2 ka, respectively) at the depth interval where the rapid increase of χ_{fd} values is observed and where the loess-soil transition has been identified in the field (Fig. S7).

A common feature of these LPS investigated in the SE European Loess Belt is a slow increase in magnetic susceptibility beginning well below the most strongly expressed Holocene soil horizons. That is, relatively minor magnetic susceptibility enhancement provides an early indication of the changing environment, before effects of other pedogenetic processes are evident.

5.2. Chinese Loess Plateau sites

For Caoxian, NW Chinese Loess Plateau, the χ_{lf} values are constant until 3.5 m, dated at 15 ka, after which they start to increase very slowly. From around 11.7 ka until ~3 ka at 1.725 m depth the increase is accelerated, after which the values remain stable until 0.3 ka at 0.725 m (Fig. 8). The visual loess-soil transition as identified in the field around 3 m has been dated to around 14 ka (Fig. 8 and S9). For Baicaoyuan (BCY), also from NW Chinese Loess Plateau the χ_{lf} values are constant from 17 ka until a sharp increase starting at 11.7 ka up to a stable level around 7 ka; there is an abrupt fluctuation early in this sharp increase (Fig. 9). Prior to 11.7 ka the intensity of the magnetic susceptibility signals are similar to those of Late Glacial loess at the Caoxian site but after 11.7 ka they are much higher, which indicates more intense pedogenesis at the Baicaoyuan site. In the context of the NW-SE gradient in the intensity of the magnetic susceptibility signal in soils across the Chinese Loess Plateau (Maher et al., 2003; Dong et al., 2015) the maximum χ_{lf} values obtained for Baicaoyuan are rather common for the sites located in the NW Chinese Loess Plateau. Across the depth interval (1.175–1.025 m) where the onset of sudden increase in χ_{lf} is identified, three OSL samples indicate continuous dust deposition. The three OSL samples above this interval also indicate ongoing loess sedimentation into the late Holocene. Taken together, these observations cast doubt on interpretations of the abrupt increase as either the result of an erosional event or a weathering front developed under intense top-down pedogenesis. The maximum χ_{lf} values at Baicaoyuan do not indicate unusually intense pedogenesis for the region of this site and OSL ages support ongoing sedimentation rather than long-lasting stability of the land surface which led to top-down pedogenesis. With that background, the abrupt χ_{lf} increase may simply record a particularly strong response of magnetic susceptibility to climatic change around 11.7 ka. The transition from loess to soil as identified in the field around 1.3 m is dated at ~14 ka, a few cm below the depth where the onset of the increase in χ_{lf} occurs (Fig. S10). Thus, at both the Chinese Loess Plateau LPS, the initial increase of magnetic susceptibility coincides with or is slightly above other evidence of pedogenesis in the lowest part of the Holocene soil.

5.3. Great Plains loess, United States

At the Kuma site (KUM), Nebraska, for the lowermost 1.4 m of loess the OSL ages do not increase with depth and scatter around 13–14 ka (Fig. 10), a common observation in the uppermost Late Pleistocene Peoria Loess in western Nebraska, and probably reflecting very high accumulation rates (Roberts et al., 2003; Mason et al., 2008). The χ_{fd} values remain relatively constant with small variations until the upper part of this depth interval when they start to slowly increase. Around 11.7 ka at 0.53 m the amplification is accelerated reaching a maximum around 8.4 ± 0.6 ka at 0.24 m and decreasing afterwards. The transition from loess to soil identified in the field occurs at around 1 m at 14 ka (Fig. S12), approximately coinciding with the initial rise in magnetic susceptibility.

To summarize, we identified a gradual and smooth increase in the magnetic susceptibility values over the loess-soil transition at seven sites (PRI, MV, RS, MVS, SM, CX and KUM) spread across the mid-latitude loess belts on three continents. The OSL chronologies indicate continuous dust accumulation and coupled with the magnetic susceptibility variation provide evidence for accretional Holocene soil formation in these sites. In two sites from SE Europe and Chinese Loess Plateau the variation in magnetic susceptibility is sharp (ROX, BCY) and in one of them (ROX), a significant OSL age hiatus is detected at the same depth. However, the luminescence ages in the soil horizons indicate dust accumulation during the Holocene.

6. Modeled mean accumulation rates

The factors that control dust deposition and settling include atmospheric turbulence, the characteristics of the particles transported by wind which are controlled by the potential source areas, and the nature of the surface where the dust settles, more specifically the topography and vegetation cover and precipitation rate (Újvári et al., 2016). Based on an assumption of accretionary pedogenesis, though recognizing greater uncertainty about that at some sites than others, dust accumulation rates are modeled in the soils as well as in the underlying loess (Fig. 11).

At most of the sites studied, accumulation rates are higher in loess, below the increase in magnetic susceptibility, and are lower in the soils, but there are several exceptions (Fig. 11). That is, the calculated accumulation rates are consistent with the hypothesis that slow sedimentation played a role in enhancing the effectiveness of Holocene pedogenesis in some, but not all, cases.

6.1. Southeastern European belt sites

At Kurortne accumulation rates are similar in Last Glacial Maximum loess and soil units, with no change across the boundary from darker AB horizons to much less pedogenically altered loess below. Low values of accumulation rates after 17 ka of 3.3 ± 0.2 cm ka^{-1} were obtained by modeling luminescence ages. At Roxolany the sediments above the

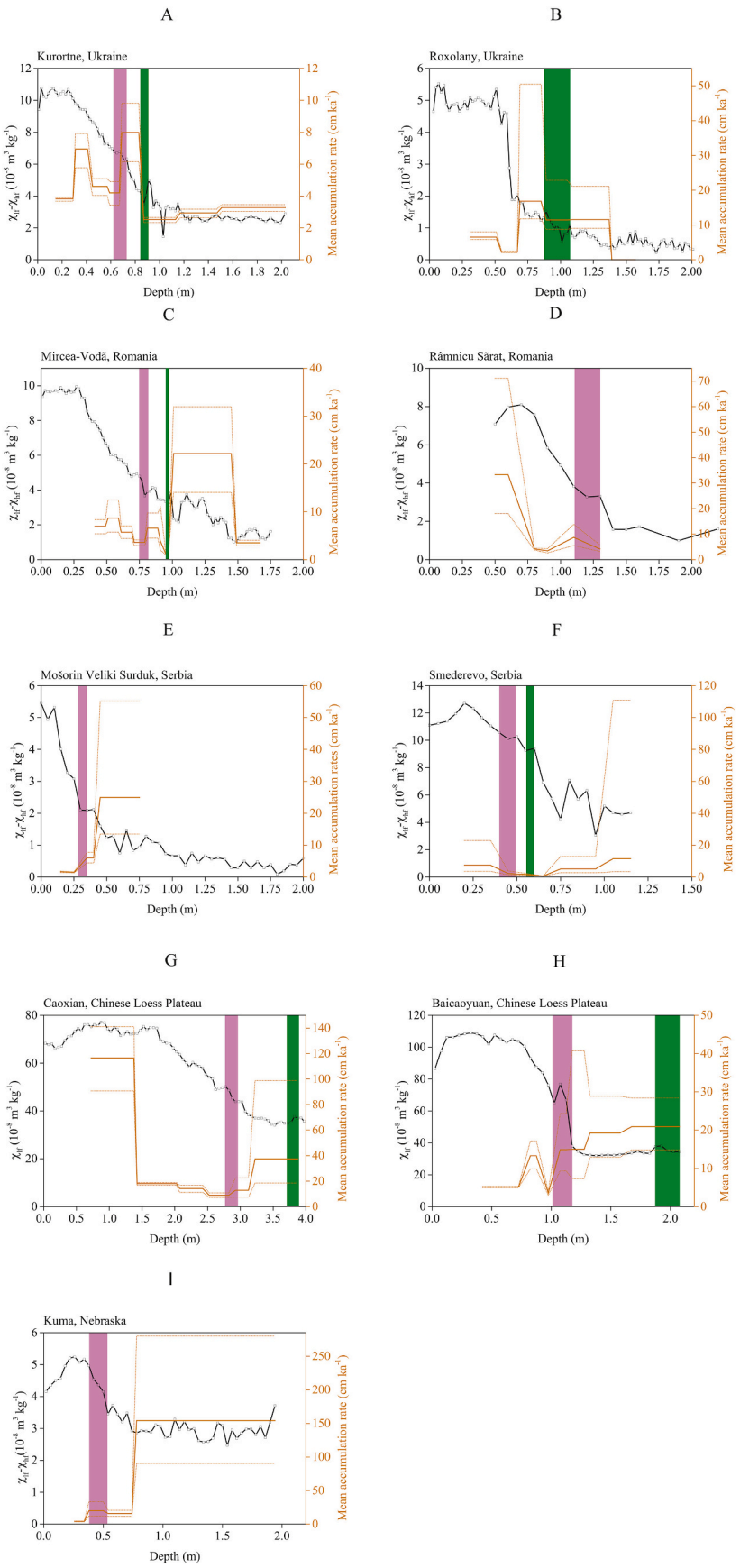

Fig. 11. A–I. Modeled accumulation rates and frequency dependent magnetic susceptibility signals plotted against depth. Note that the low frequency magnetic susceptibility signal is represented for Caoxian and Baicaoyuan sites. 1 sigma uncertainties of the sedimentation rates are given with dotted lines. The time intervals covering 11.7 ka and 17.5 ka are hachured with light and dark colour, respectively.

depth where the age gap is identified, after 8.6 ± 0.7 ka, accumulated at a mean rate of 7 cm ka^{-1} (Fig. 11B) which is comparable to accumulation rates in the other SE European sites that display a smooth increase in χ_{fd} values. The very low apparent accumulation rate at the base of the soil in this LPS (Fig. 3) results from the age jump there at about the same depth as the abrupt increase in magnetic susceptibility, both most plausibly explained by an erosional discontinuity rather than a climatic event. In the loess below the discontinuity mean accumulation rates are higher than in the soil, 17 cm ka^{-1} and 7 cm ka^{-1}, respectively.

At Mircea Voda, around 17 ka the luminescence ages indicate a decrease in the mean accumulation rate near the base of the soil profile (Figs. 4 and 11C). The mean accumulation rates after 17 ka vary from 4 to 9 cm ka^{-1}. The magnetic susceptibility increase at this site begins prior to the change in accumulation rate but most of the increase occurs under conditions of slow accumulation. At Ramnicu Sarat, minimum mean accumulation rates after 11.7 ka reach 6 cm ka^{-1} (Fig. 11D), similar to those in soils at most other sites. A higher accumulation rate is calculated for the three uppermost samples within the soil, accompanied by some decrease in magnetic susceptibility as noted above. Due to strong inversions for ages older than 12 ka we were unable to calculate reliable accumulation rates. At Mošorin Veliki Surduk, the mean accumulation rates diminish after 14 ka to a minimum of 2 cm ka^{-1}. Most increase in magnetic susceptibility occurs after the shift to slower accumulation (Fig. 11), which occurs near the base of the soil (Fig. 6). Finally, at Smederevo, the mean accumulation rate is similar for loess and soil units varying from 5 to 7 cm ka^{-1}, and the increase in magnetic susceptibility is not associated with slower accumulation (Fig. 11).

6.2. Chinese Loess Plateau and Great Plains Sites

At all three of these LPS, accumulation rates decreased from underlying loess into the soils. At Caoxian the modeled accumulation rates decrease in transitional horizons between unweathered loess and more pedogenically altered horizons (Figs. 8 and 11). The calculated sediment rate increases to higher values again in the late Holocene at Caoxian. At Baicaoyuan, mean accumulation rates reduce after 11.7 ka well above the base of the Holocene soil (Figs. 11H and 9). These are similar to the values obtained for Caoxian site as well as the European sites. At Kuma reduction in the mean accumulation rate occurs around 14 ka, as well (Fig. 11 I). While the accumulation rate in the loess below the soil at Kuma is higher compared to other sites, this is expected for the central Great Plains (Roberts et al., 2003). At all three of these sites both the stratigraphy and the OSL chronology demonstrated a continuous record of dust deposition, though at varying rates, that competed with pedogenesis from the Late Pleistocene through the Holocene.

7. Discussion

7.1. Timing of the initiation and acceleration of the magnetic susceptibility enhancement in loess deposits

In the majority of the investigated sites the onset of magnetic susceptibility enhancement was dated prior to 11.7 ka, as early as 14–17.5 ka (Kurortne, Roxolany, Ramnicu Sarat, Mošorin, Caoxian and Kuma; Figs. 2, 3, 5, 6, 8, 10) or even earlier (Mircea Voda and Smederevo; Figs. 4, 7). At one site the magnetic susceptibility signal starts to increase sharply around 11.7 ka (Baicaoyuan; Fig. 9). Furthermore, the rate of increase in magnetic susceptibility accelerates around 11.7 ka at some but not all of these sites, (Kurortne, Mircea Voda, Mošorin, Caoxian and Kuma; Figs. 2, 4, 6, 8, 10).

Here we assume that the start of the Pleistocene-Holocene climatic transition produces the onset of magnetic susceptibility signal amplification in the investigated loess deposits. Based on the luminescence ages, the transition occurs prior to 11.7 ka, as early as 14–17.5 ka. Thus, in some sites, it is concurrent with the timing of the most rapid global sea-level rise event, Meltwater Pulse 1A (MWP-1A) dated to 14.7 ka (Lin et al., 2021). Also, it generally agrees with Termination 1 in benthic $\delta^{18}O$ records in North Atlantic dated to 17.5 ka (Stern and Lisiecki, 2014). However, it shall be stated that Khider et al. (2017) discussed much larger temporal variability (13–20 ka) for Termination 1 as dated in several tropical sea-surface temperature records.

Since χ_{lf} is influenced by the bulk mineralogy's magnetic properties, but χ_{fd} is controlled only by the superparamagnetic fraction, these two magnetic parameters react differently to translocation and leaching processes. Taking into account that the same trend can be observed in both χ_{lf} and χ_{fd}, we think that they were not significantly influenced by top-down soil development.

7.1.1. Comparison with absolute ages reported for Chinese Loess Plateau

In the Yuanbao loess section, located in the western CLP, based on quartz luminescence ages, Lai and Wintle (2006) date the onset and acceleration of magnetic susceptibility enhancement to ~15 ka and ~ 9.8 ka, respectively. They place the Pleistocene-Holocene climatic transition based on the changes in the sensitivity of the luminescence signals in quartz and report an age of ~13 ka.

At the Beiguoyuan, Xifeng, Xunyi, and Shiguanzhai loess sections, distributed across the CLP from north to south, it is more difficult to accurately date the initial increase in magnetic susceptibility, because the start of this increase falls within intervals in which luminescence ages are scattered with inversions and/or display gaps interpreted as hiatuses (Lu et al., 2006; Stevens et al., 2006, 2007, 2008). These intervals cover various intervals between 20 ka and < 10 ka, with ages differing between sites. Similarly, at Luochuan site, in the central CLP, at the depth interval where the onset of magnetic susceptibility enhancement occurs, high-resolution (10 cm) luminescence ages suddenly jump to ~17 ka, yielding a ~ 6 ka age gap across 50 cm (Lu et al., 2013).

The timing and smoothness of magnetic susceptibility increase at Caoxian are similar to the Yuanbao site and the ~14 ka date reported there. A close resemblance in the magnetic susceptibility signal intensity of the glacial loess (~ 30 $10^{-8}m^3kg^{-1}$) and soil (60–70 $10^{-8}m^3kg^{-1}$) can be seen between Caoxian, (western CLP) and Huanxian (central-north CLP) (Dong et al., 2015) that display much lower values compared to Yuanbao, 50 $10^{-8}m^3kg^{-1}$ and 170 $10^{-8}m^3kg^{-1}$ for loess and soil, respectively.

Baicaoyuan appears similar to Yuanbao only in terms of magnetic susceptibility signal intensities of 50 $10^{-8}m^3kg^{-1}$ and 170 $10^{-8}m^3kg^{-1}$ for loess and soil, respectively. The increase in magnetic susceptibility is much more abrupt at Baicaoyuan and also displays a short-term fluctuation early in the increase. A similar short-term fluctuation is evident at Luochuan, but occurs later, in the early Holocene (Lu et al., 2013).

Dong et al. (2015) noted relatively abrupt shifts in the magnetic susceptibility record with ages decreasing from southeast to northwest across the plateau (~11 ka to ~7 ka). They attribute the time transgressive nature of this shift to the gradual strengthening of the Asian Summer Monsoon (ASM) and the consequent changes in precipitation to which the magnetic susceptibility signal is sensitive. In this study, the luminescence ages on the two investigated sites in the western CLP reveal a relatively small inverse gradient with the ages increasing from ~11.7 ka (± 1 ka) in Baicaoyuan (farther south) to ~14 ka (± 1 ka) in Caoxian (farther north) for the onset of magnetic susceptibility increase.

This comparison with results of previous research demonstrates significant remaining issues in establishing the timing of the Pleistocene-Holocene climatic transition as recorded by magnetic susceptibility in the CLP. At both Yuanbao (Lai and Wintle, 2006) and the Caoxian LPS sampled for this study, luminescence dating indicates relatively continuous records through the interval 10–15 ka and magnetic susceptibility increases gradually with the increase beginning at 15–13 ka. At several other sites, the luminescence chronology indicates hiatuses covering the interval 10–15 ka; these records do not confirm initiation of the increase in magnetic susceptibility at 15–13 ka but apparently do not rule it out (e.g. Stevens et al., 2008, Fig. 19–20 therein). The Baicaoyuan LPS also has a luminescence chronology indicating continuous

sedimentation but displays a more abrupt and later initial increase of magnetic susceptibility than at Caoxian and Yuanbao. This contrast likely reflects some local variation in Pleistocene-Holocene environmental change but cannot be further explained without data from additional sites with continuous records through the key time interval.

7.1.2. Comparison with previous research in the south-eastern European loess belt

To our knowledge, the literature lacks high resolution OSL studies on the Pleistocene-Holocene climatic transition recorded in the European loess sites. Generally, there is a good agreement between our results and the ones previously reported. Based on one quartz OSL age the magnetic susceptibility starts to increase before 13 ± 1 ka in Orlovat site (Marković et al., 2014; Timar-Gabor et al., 2015) and around 13 ± 1 ka in Crvenka, Middle Danube Basin (Stevens et al., 2011; Marković et al., 2018). However, at Surduk, in the same region, a very young ^{14}C age of 7.3 ± 0.38 cal ka BP (Hatté et al., 2013) is reported for the onset of magnetic susceptibility enhancement. A quartz OSL age of 11 ± 1 ka is reported above the area of magnetic susceptibility enhancement in Lunca (Constantin et al., 2015) and Urluia (Fitzsimmons and Hambach, 2014) in the Lower Danube Basin. Regarding the Black Sea loess region in Ukraine, magnetic susceptibility investigations have been carried out by Nawrocki et al. (1999) and Bakhmutov et al. (2017), among others, but this area lacks reliable numerical dating.

7.1.3. Comparison with previous research in the Central Great Plains

The Pleistocene-Holocene climatic transition in the Central Great Plains (Nebraska and Kansas) is expressed stratigraphically by the transition from Peoria Loess deposited ca. 28 ka to about 14–13 ka during the last glacial (late Wisconsin) period, to the dark, organic rich buried Brady Soil (Johnson and Willey, 2000; Roberts et al., 2003; Mason et al., 2008; Schaetzl et al., 2018). After Brady soil formation, accelerated dust deposition during Holocene formed Bignell loess (Mason et al., 2003). Across large areas of the central Great Plains that are farther from Holocene loess sources, the Brady Soil is at <1 m depth and has often been transformed into a horizon of the modern soil through accretional pedogenesis (Jacobs and Mason, 2007).

The new dating results reported here from the Kuma LPS are consistent with extensive OSL and radiocarbon dating of the Brady Soil (Johnson and Willey, 2000; Mason et al., 2003; Roberts et al., 2003; Miao et al., 2007; Mason et al., 2008; Tecsa et al., 2020b). This prior work indicates the uppermost Peoria Loess was deposited rapidly at 14–15 ka. OSL ages just below the lower A horizon of the Brady Soil range from 12.6 to 15.8 ka, with most between 13 and 15 ka, while OSL ages just above the Brady Soil are mostly between 9 and 10 ka. Radiocarbon ages are largely consistent with the OSL dating, including paired radiocarbon and OSL ages at 10 cm intervals in the Old Wauneta Roadcut, reported by Mason et al. (2008). Tecsa et al. (2020b) applied OSL dating based on multiple grain sizes of quartz, as used in the present study, to the Enders LPS, dating the base of the Brady Soil to 13.1 ± 0.8 ka and the top of it to 9.5 ± 0.6 ka.

The increase in magnetic susceptibility to a peak in the Brady Soil is well-defined at the Kuma LPS and at some sites previously studied by Johnson and Willey (2000). A calibrated radiocarbon age of 13.3 ka near the start of the increase in χ_{lf} at the Beisel-Steinle site of Johnson and Willey (2000) is not much younger than the age of ~14 ka at this point in the Kuma LPS, but at two of those authors' other sites where there is χ_{lf} enhancement near the base of the Brady Soil, radiocarbon ages are anomalously young relative to the regional record. In other LPS of this region, magnetic susceptibility does not display such a well-defined peak in the Brady Soil (Johnson and Willey, 2000; Miao et al., 2007; Tecsa et al., 2020b).

Other proxy data are consistent with environment change at about the time of the initial increase in magnetic susceptibility at Kuma at ~14 ka. At the Enders LPS, the shift toward finer particle size that characterizes the Brady Soil begins below an age of 13.1 ka and about 20 cm above an age of 14.0 ± 0.9 ka (Tecsa et al., 2020b), though higher in the Brady Soil, particle size variation is more complex than the profile of magnetic susceptibility at Kuma. Also at Enders LPS, a major shift toward higher $\delta^{13}C$ of carbonates begins at a similar depth as the shift to finer particle size and is tentatively interpreted as indicating growing abundance of C_4 grasses with warming temperature (Tecsa et al., 2020b), based on correlation with carbon isotopic records from organic matter at nearby sites (Feggestad et al., 2004; Miao et al., 2007). All of these proxies are likely to record specific aspects of Pleistocene-Holocene environmental change, with different temporal patterns corresponding to the specific factors they respond to.

7.2. Accretional soil formation in loess regions and implications for interpreting loess records

Luminescence ages that decrease steadily upward through a soil are consistent with ongoing sedimentation and accretional soil development. However, forms of mixing such as bio- or cryoturbation can potentially also yield similar luminescence age trends through the downward transport of soil exposed to light at the ground surface. Bateman et al. (2003) presented the scenario of a slowly aggrading surface or deposition of thin sedimentary packages, resulting in OSL ages younger than the time of deposition. Bateman et al. (2003) also reported empirical evidence on the complex effects of pedoturbation on OSL ages and on the heterogeneity of single aliquots and single grain quartz OSL data. Johnson et al. (2014) report an "apparent" decrease in young OSL ages with increasing depth produced from a purely pedogenic, nondepositional model. They present single-grain quartz OSL ages in combination with a modeled age-tracer that is capable of simulating realistic soil mixing. Gray et al. (2020) also modeled depth trends of D_e produced in soils by pedoturbation without ongoing sedimentation.

Because of the possible effects of mixing processes on OSL age trends within soils, we closely examined the data available from luminescence measurements that can indicate the extent of mixing or at least a difference in the amount of mixing between soils and the loess they formed in. In this study, the observation of low (<20%) overdispersion in luminescence data from soil horizons, and similar low overdispersion in soils as in loess-soil transition zones and underlying loess, fully supports the interpretation of accretional pedogenesis for the Chinese Loess Plateau and Great Plains sites. In the SE European LPS this interpretation is more debatable because the overdispersion values up to 30% in soil horizons at the Mircea Voda and Kurortne LPS (Table 1) might indicate that the top-down soil formation has affected ages within the soils at those sites. Constantin et al. (2019, Fig. S7 therein) report overdispersion values indicating little difference between soils and underlying loess at some other SE European sites, however.

Beyond the luminescence data, the interpretation of Holocene accretional pedogenesis is supported by the observation that many of the Holocene ages in these LPS—including those in SE Europe—fall within subsurface soil horizons, not in a thick and homogeneous A horizon consistent with deep mixing from the surface downward (Figs. 2–10). In the Kurortne, Mircea Voda, Ramnicu Sarat, Baicaoyuan, and Kuma LPS, Holocene ages fall along age-depth trends of relatively consistent slope across multiple distinctly different horizons (Figs. 2, 4, 5, 10), also more readily explained by sedimentation than by deep mixing. On the other hand, the Holocene soil in the SE European sites appears to have more strongly expressed horizons than at the Great Plains and Chinese Loess Plateau sites. This contrast could indicate stronger top-down processes at the SE European loess sites, though it could also reflect a difference in climate and other factors influencing in pedogenesis. In the Great Plains, more strongly expressed soil profiles are common in more humid central Nebraska than at the Kuma LPS, yet Jacobs and Mason (2007) presented a range of evidence for accretionary formation of the more strongly expressed soils as well as profiles like the Kuma LPS where the burial of the Brady Soil by Holocene dust sedimentation is more evident.

Overall, our data clearly support the dominance of accretional

pedogenesis resulting from ongoing Holocene dust deposition in the Chinese Loess Plateau and Great Plains LPS. In fact, both regions are characterized by historical and modern dust storms with climatic as well as land-use related drivers (Sun et al., 2001; Lee and Gill, 2015). For the SE European LPS we conclude that the OSL ages reflect Holocene dust deposition, but the balance between accretionary and top-down soil formation is still debatable and additional research is needed on this issue.

Regardless of the exact balance, our interpretation of the Holocene soils in these LPS does not correspond to the scenario of ceased dust deposition during interstadials employed by Rousseau et al. (2017, 2021) in their conceptual models for soil development in loess. It is possible that the competition between top-down soil development and dust accretion is different at sites we studied than at central and western European sites, much more strongly influenced by millennial-scale climate changes related to variations in the Atlantic Meridional Overturning Circulation (AMOC) allowing for periods of increased precipitation.

With that background we can consider the implications of accretionary pedogenesis at our study sites for the soils now observed there and for the magnetic enhancement of these soils in particular. As discussed in previous research on accretional soils (e.g. McDonald and Busacca, 1990; Almond and Tonkin, 1999; Jacobs and Mason, 2007; Kemp, 2001), each new increment of dust is added at the surface where a specific set of pedogenetic processes are most effective, and then is progressively buried and in effect moved into the shallow subsurface. It can be altered there by the conditions and processes characteristic of soil B horizons but eventually, through ongoing burial it can reach a point where it is no longer significantly affected by pedogenesis. In other words, dust added at the surface is incorporated into an upbuilding A horizon, while at the same time, an earlier-formed part of the A horizon may be losing organic matter and acquiring a colour and structure more characteristic of B horizons and eventually may move to a depth where pedogenetic processes are much less effective. Jacobs and Mason (2007) describe this process for many sites in the central Great Plains, mostly farther east and in more humid environments than the Kuma LPS. Importantly though, the specific transformations that take place must be related to the environmental conditions and rate of dust accumulation. Rapid accumulation in a cold, dry environment, often inferred for Late Pleistocene loess, allows only minor alteration in the near-surface (e.g. root traces, subtle biogenic and/or cryogenic structures visible in thin sections, etc.) before deep burial (Kemp et al., 1995; Kemp, 2001). In contrast, in the Holocene environments of all of the studied LPS, dust accumulating at rates of <10 cm ka^{-1} would have been more substantially altered by organic matter accumulation, soil structure formation, and other pedogenetic processes quickly enough to allow the soil grow upward over time. The degree of transformation of horizons as they are progressively buried can still vary with the local environment and rate of dust accumulation. At the Kuma LPS, the Brady Soil has been buried by Holocene dust, but still retains many characteristics of an A horizon. At the SE European LPS, if our interpretation of Holocene dust accumulation is correct, current B horizons were once at the land surface and could have had characteristics of A horizons.

Magnetic susceptibility records in LPS can be interpreted in light of these general features of accretional pedogenesis (Jordanova and Jordanova, 2020, 2021). We start here with the initial increase in magnetic susceptibility we use to date the Pleistocene-Holocene climatic transition. Field observations at some study sites reveal increasing evidence of pedogenesis associated with increasing magnetic susceptibility, including redder hues and progressively darker colors probably reflecting greater organic matter content (Figs. 2–10). At other sites the initial increase in magnetic susceptibility occurs below evidence of incipient pedogenesis that is clearly visible in the field. In either case, it is likely that increased magnetic enhancement is an early response to changing climate. In fact, Jordanova and Jordanova (2021) conclude that the minimum susceptibility observed in loess below soil profiles includes some enhancement that occurred under glacial climate conditions.

Assuming accretional pedogenesis, the simplest explanation of a gradual, smooth upward increase in magnetic susceptibility near the base of the Holocene soil is a gradually more humid and warmer climate increasing the degree of magnetic susceptibility enhancement and pedogenesis in general. We do not attempt more specific interpretation of the climatic change represented by the magnetic susceptibility record at these study sites, recognizing the many factors that may influence it. These include the role of local topography (Brantley et al., 2017), organic matter (Lawrence et al., 2014), grain size on chemical weathering rates as well as the changing rate of soil formation over time (Egli et al., 2018), the soil type (Hanesch and Scholger, 2005). See Jordanova and Jordanova (2021) for a recent comprehensive analysis of European and Chinese profiles, in which both the minimum magnetic susceptibility signal of last glacial loess and pedogenic magnetic susceptibility of Holocene soils display multilinear relationships with both present day mean annual precipitation and mean annual temperature values at corresponding locations. Strong deviations from these relationships may be related to local effects such as coarse grain size.

Along with climatic change, a decreasing accumulation rate at some but not all of our study sites could possibly contribute to the trends of increasing magnetic susceptibility and increasing field evidence of pedogenesis. Slower accumulation means that the accumulating sediment is kept within the near-surface zone of most effective pedogenesis for more time (Roberts, 2008; Schaetzl and Anderson, 2009). In any case, a decreased accumulation rate, especially when observed across a large region, will itself often reflect climatic change reducing rates of dust emission and transport.

A more abrupt increase in magnetic susceptibility clearly could record a response to rapid climate change (Landais et al., 2018) but could have at least three other explanations. There could be a discontinuity in the record reflecting erosion or lack of sedimentation, or there may have been some downward progression of pedogenic processes including magnetic enhancement in the initial stages of accretional soil formation (Jordanova and Jordanova, 2020). The later would seemingly cause an age offset in case pedogenesis (i.e., magnetic susceptibility enhancement) alone is taken as paleoclimate proxy. The third possibility could be relative increases in magnetic susceptibility due to carbonate mineral dissolution at the carbonate weathering front, which can be ruled out by measurement of the frequency-dependent susceptibility.

As the climatic transition continued and the accumulation rate decreased at many of the studied LPS, pedogenetic processes became more pronounced. In LPS of the Chinese Loess Plateau and the Great Plains, and at some of the Southeastern European sites, this process continued into the Holocene, resulting in a relatively thick sequence of primarily A and AB horizons with varying degrees of structural development and organic matter accumulation. Pedogenetic carbonate accumulation likely formed below the currently active surface A horizon, overprinting deeper horizons formed earlier in the accretional process (supported by isotopic data from carbonates and organic matter at loess sections near Kuma, Tecsa et al., 2020b). It is possible that some deeper horizons originated as A horizons but now resemble B horizons because of post-burial loss of organic matter and structural changes, especially in the Southeastern European LPS. At sites in the Chinese Loess Plateau and Great Plains, more weakly developed, lighter-colored upper horizons reflect change to a drier climate later in the Holocene.

The magnetic susceptibility profiles within the soil at our study sites are varied, and here we do not attempt an interpretation of these profiles in terms of Holocene climatic change, ongoing dust sedimentation, and any significant component of top-down pedogenesis. Jordanova and Jordanova (2020) review the issues involved in detail.

If this conceptual model is accurate and applies more generally to LPS spanning the Pleistocene-Holocene transition, then it is valid to interpret vertical profiles of not only magnetic parameters, but also isotopic composition of organic matter (e.g. Miao et al., 2007) as

essentially time series produced by steady upbuilding of the land surface by dust deposition. The same could be true of carbonate isotopic composition (e.g. Tecsa et al., 2020b) and other pedogenetic properties and features, though more research is needed to assess the depth range over which they form in these accretional soils. Some "smearing" of these records must be acknowledged, because magnetic enhancement and organic matter addition both occur over a zone of some thickness below the ground surface, and because bio- or cryoturbation likely always have at least minor effects over some depth scale. However, in a semiarid steppe environment where deeper horizons are rarely wetted, these records are probably locked in after burial to sufficient depth.

8. Conclusions

In this study we have measured at very high-resolution the magnetic susceptibility record across the transition from the last glacial loess to the Holocene soil in nine sites from the Chinese Loess Plateau, southeastern European loess-belt and central Great Plains, Nebraska, USA. In all sites but two (Baicaoyuan and Roxolany) the magnetic susceptibility signal increases gradually. We have placed the onset of the magnetic susceptibility enhancement at the depth where the χ_{fd} values increase significantly and continuously compared to those values that characterize the late glacial loess (or where available LGM loess) following the approach of Stern and Lisiecki (2014) for the oxygen isotope chronology in marine sediments.

Using high-resolution luminescence dating on multiple grain-size fractions of quartz we dated the onset of magnetic susceptibility enhancement and consequently the onset of Pleistocene-Holocene climatic transition recorded in Chinese Loess Plateau, southeastern European loess belt and central Great Plain loess deposits prior to 11.7 ka, around 14–17.5 ka. Thus, we conclude that the onset of the Pleistocene-Holocene climatic transition recorded in loess deposits by the magnetic susceptibility signal is not synchronous among all of the investigated sites from Chinese Loess Plateau, southeastern European belt and central Great Plains, Nebraska, USA. The timing of this transition generally agrees, however, with the ~17.5 ka date for Termination 1 in oxygen isotopes record in marine sediments from North Atlantic reported by Stern and Lisiecki (2014) and to the global sea-level rise event Meltwater Pulse 1A dated to 14.7 ka (Lin et al., 2021).

The detailed luminescence chronology points to more or less continuous dust accumulation during the Pleistocene-Holocene transition as well as into the Holocene at the investigated sites in SE Europe, China and US. Coupled with other evidence it indicates that dust sedimentation and pedogenesis act simultaneously and result in a non-negligible accretional component in the formation of Holocene soils at the sites investigated, with important implications for the interpretation of magnetic susceptibility and other paleoclimatic proxies. This conclusion is more definite for the sites in the Chinese Loess Plateau and Great Plains, and less so for the SE European sites. While accretional pedogenesis has often been implicitly or explicitly assumed in paleoclimatic interpretation of loess-paleosol sequences, especially in the Chinese Loess Plateau, our luminescence data add direct evidence for ongoing sedimentation as soils formed. The high resolution luminescence ages allowed modeling of accumulation rates for the Holocene soil that are similar for European, Chinese and US loess sites investigated here and vary between 2 cm ka^{-1} to 9 cm ka^{-1}.

Our results highlight the need of combining absolute dating with high-resolution paleoclimatic proxies (e.g. magnetic susceptibility) to accurately estimate the timing of the Pleistocene-Holocene climatic transition from these complex records produced by dust accumulation and accretional pedogenesis. Presented results indicate diverse environmental dynamics recorded in the different North Hemisphere loess regions during the major global climatic shift such as the transition from the last glacial to the Holocene. Understanding of these asynchronous responses of the terrestrial ecosystem to past global climate changes is important for adequate interpretations of current and prediction of future interactions between climatic and environmental evolution.

Supplementary data to this article can be found online at https://doi.org/10.1016/j.earscirev.2021.103769.

Author's contribution

Daniela Constantin: Methodology, Data curation, Formal Analysis, Visualization, Writing - original draft, Writing - review & editing. **Joseph Mason:** Methodology, Visualization, Writing - original draft, Writing - review & editing. **Daniel Veres:** Methodology, Investigation, Formal Analysis, Writing - original draft, Writing - review & editing. **Ulrich Hambach:** Methodology, Writing - original draft, Writing - review & editing. **Cristian Panaiotu:** Methodology, Investigation, Formal Analysis, Visualization, Writing - original draft, Writing - review & editing. **Christian Zeeden:** Formal Analysis, Writing - original draft. **Liping Zhou:** Formal Analysis. **Slobodan Marković:** Investigation, Writing - original draft. **Natalia Gerasimenko:** Investigation, Writing - original draft. **Anca Avram, Viorica Tecsa, Ștefana-Mădălina Groza-Sacaciu:** Investigation. **Laura del Valle Villalonga:** Investigation, Visualization. **Robert Begy:** Investigation. **Alida Timar-Gabor:** Conceptualization, Funding acquisition, Methodology, Investigation, Writing - original draft, Writing - review & editing, Supervision.

Declaration of Competing Interest

The authors declare that they have no known competing financial interests or personal relationships that could have appeared to influence the work reported in this paper.

Acknowledgements

This study has received funding from the European Research Council (ERC) under the European Union's Horizon 2020 research and innovation programme ERC-2015-STG, (grant agreement No [678106]). Comments from three anonymous reviewers have improved the paper.

References

Aitken, M.J., 1976. Thermoluminescent age evaluation and assessment of errorlimits: revised system. Archaeometry 18, 233–238. https://doi.org/10.1111/j.1475-4754.1976.tb00168.x.

Aitken, M.J., 1985. Thermoluminescence Dating. Academic Press, London.

Aitken, M.J., Alldred, J.C., 1972. The assessment of error limits inthermoluminescent dating. Archaeometry 14, 257–267. https://doi.org/10.1111/j.1475-4754.1972.tb00068.x.

Albani, S., Mahowald, N.M., Winckler, G., Anderson, R.F., Bradtmiller, L.I., Delmonte, B., François, R., Goman, M., Heavens, N.G., Hesse, P.P., Hovan, S.A., Kang, S.G., Kohfeld, K.E., Lu, H., Maggi, V., Mason, J.A., Mayewski, P.A., McGee, D., Miao, X., Otto-Bliesner, B.-L., Perry, A.T., Pourmand, A., Roberts, H.M., Rosenbloom, N., Stevens, T., Sun, J., 2015. Twelve thousand years of dust: the Holocene global dust cycle constrained by natural archives. Clim. Past 11, 869–903. https://doi.org/10.5194/CP-11-869-2015.

Almond, P.C., Tonkin, P.J., 1999. Pedogenesis by upbuilding in an extreme leaching amd weathering environment, and slow loess accretion, South Westland, New Zealand. Geoderma 92, 1–36. https://doi.org/10.1016/S0016-7061(99)00016-6.

Bakhmutov, V.G., Kazansky, A.Y., Matasova, G.G., Glavatskii, D.V., 2017. Petromagnetism and magnetostratigraphy of Ukrainian loess/palaeosol sequence (Roxolany, Boyanichi and Korshev sections). Izvestiya Phys. Solid Earth (FizikaZemli) 53, 864–884.

Bateman, M.D., Boulter, C.H., Carr, A.S., Frederick, C.D., Peter, D., Wilder, M., 2007. Preserving the palaeoenvironmental record in Drylands: Bioturbation and its significance for luminescence-derived chronologies. Sediment. Geol. 195 (1–2), 5–19. https://doi.org/10.1016/j.sedgeo.2006.07.003.

Bateman, M.D., Frederick, C.D., Jaiswal, M.K., Singhvi, A.K., 2003. Investigations into the potential effects of pedoturbation on luminescence dating. Quater. Sci. Rev. 22 (10–13), 1169–1176. https://doi.org/10.1016/S0277-3791(03)00019-2.

Bazin, L., Landais, A., Lemieux-Dudon, B., ToyéMahamadouKele, H., Veres, D., Parrenin, F., Martinerie, P., Ritz, C., Capron, E., Lipenkov, V., Loutre, M.-F., Raynaud, D., Vinther, B., Svensson, A., Rasmussen, S., Severi, M., Blunier, T., Leuenberger, M., Fischer, H., Masson-Delmotte, V., Chappellaz, J., Wolff, E., 2013. An optimized multi-proxy, multi-site Antarctic ice and gas orbital chronology (AICC2012): 120-800 ka. Clim. Past 9, 1715–1731. https://doi.org/10.5194/cp-9-1715-2013.

Bøtter-Jensen, L., Thomsen, K.J., Jain, M., 2010. Review of optically stimulated luminescence (OSL) instrumental developments for retrospective dosimetry. Radiat. Meas. 45, 253–257. https://doi.org/10.1016/j.radmeas.2009.11.030.

Brantley, S.L., Lebedeva, M.I., Balashov, V.N., Singha, K., Sullivan, P.L., Stinchcomb, G., 2017. Toward a conceptual model relating chemical reaction fronts to water flow paths in hills. Geomorphology 277, 100–117. https://doi.org/10.1016/j.geomorph.2016.09.027.

Clark, P.U., Shakun, J.D., Baker, P.A., Bartlein, P.J., Brewer, S., Brook, E., Carlson, A.E., Cheng, H., Kaufman, D.S., Liu, Z., Marchitto, T.M., Mix, A.C., Morrill, C., Otto-Bliesner, B.L., Pahnke, K., Russell, J.M., Whitlock, C., Adkins, J.F., Blois, J.L., Clark, J., Colman, S.M., Curry, W.B., Flower, B.P., He, F., Johnson, T.C., Lynch-Stieglitz, J., Markgraf, V., McManus, J., Mitrovica, J.X., Moreno, P.I., Williams, J.W., 2012. Global climate evolution during the last deglaciation. Proc. Natl. Acad. Sci. U. S. A. 109, E1134–E1142. https://doi.org/10.1073/pnas.1116619109.

Constantin, D., Camenita, A., Panaiotu, C., Necula, C., Codrea, V., Timar-Gabor, A., 2015. Fine and coarse-quartz SAR-OSL dating of Last Glacial loess in Southern. Romania. Quat.Int. 357, 33–43. https://doi.org/10.1016/j.quaint.2014.07.052.

Constantin, D., Veres, D., Panaiotu, C., Anechitei-Deacu, V., Groza, S.M., Begy, R., Kelemen, S., Buylaert, J.-P., Hambach, U., Markovic, S.B., Gerasimenko, N., Timar-Gabor, A., 2019. Luminescence age constraints on the Pleistocene-Holocene transition recorded in loess sequences across SE Europe. Quat.Geochronol 49, 71–77. https://doi.org/10.1016/j.quageo.2018.07.011.

Dearing, J.A., Dann, R.J.L., Hay, K., Lees, J.A., Loveland, P.J., Maher, B.A., O'Grady, K., 1996. Frequency-dependent susceptibility measurements of environmental materials. Geophys. J. Int. 124, 228–240. https://doi.org/10.1111/j.1365-246X.1996.tb06366.x.

Dong, Y., Wu, N., Li, F., Huang, L., Wen, W., 2015. Time-transgressive nature of the magnetic susceptibility record across the Chinese Loess Plateau at the Pleistocene/Holocene transition. PLoS One 10 (7), e0133541. https://doi.org/10.1371/journal.pone.0133541.

Duller, G.A.T., 2003. Distinguishing quartz and feldspars in single grain luminescence measurements. Radiat. Meas. 37, 161–165. https://doi.org/10.1016/S1350-4487(02)00170-1.

Egli, M., Hunt, A., Dahms, D., Raab, G., Derungs, C., Raimondi, S., Yu, F., 2018. Prediction of soil formation as a function of age using the percolation theory approach. Front. Environ. Sci. 6, 1–21.

Feggestad, A.J., Jacobs, P.M., Miao, X., Mason, J.A., 2004. Stable carbon isotope record of Holocene environmental change in the central Great Plains. Phys. Geogr. 25, 170–190. https://doi.org/10.2747/0272-3646.25.2.170.

Fitzsimmons, K.E., Hambach, U., 2014. Loess accumulation during the last glacial maximum: evidence from Urluia, southeastern Romania. Quat. Int. 334-335, 74–85. https://doi.org/10.1016/j.quaint.2013.08.005.

Galbraith, R.F., Roberts, R.G., 2012. Statistical aspects of equivalent dose and error calculation and display in OSL dating: an overview and some recommendations. Quat.Geochronol 11, 1–27. https://doi.org/10.1016/j.quageo.2012.04.020.

Galbraith, R.F., Roberts, R.G., Laslett, G.M., Yoshida, H., Olley, J.M., 1999. Optical dating of single and multiple grains of quartz from Jinmium rock shelter, northern Australia: part I, experimental design and statistical models. Archaeometry 41, 339–364. https://doi.org/10.1111/j.1475-4754.1999.tb00987.x.

Gliganic, L.A., May, J.-H., Cohen, T.J., 2015. All mixed up: using single-grain equivalent dose distributions to identify phases of pedogenic mixing on a dryland alluvial fan. Quat. Int. 362, 23–33. https://doi.org/10.1016/j.quaint.2014.07.040.

Govin, A., Capron, E., Tzedakis, P.C., Verheyden, S., Ghaleb, B., Hillaire-Marcel, C., St-Onge, G., Stoner, J.S., Bassinot, F., Bazin, L., Blunier, T., Combourieu-Nebout, N., El Ouahabi, A., Genty, D., Gersonde, R., Jimenez-Amat, P., Landais, A., Martrat, B., Masson-Delmotte, V., Parrenin, F., Seidenkrantz, M.-S., Veres, D., Waelbroeck, C., Zahn, R., 2015. Sequence of events from the onset to the demise of the last Interglacial: evaluating strengths and limitations of chronologies used in climatic archives. Quater. Sci. Rev. 129, 1–36. https://doi.org/10.1016/j.quascirev.2015.09.018.

Gray, H.J., Keen-Zebert, A., Furbish, D.J., Tucker, G.E., Mahan, S.A., 2020. Depth-dependent soil mixing persists across climate zones. PNAS 117, 8750–8756. https://doi.org/10.1073/pnas.1914140117.

Groza-Sacaciu, S.-M., Panaiotu, C., Timar-Gabor, A., 2020. Single Aliquot Regeneration (SAR) Optically stimulated luminescence dating protocols using different grain-sizes of quartz: revisiting the chronology of MirceaVoda loess-paleosol master section (Romania). Methods Protocols 3, 19. https://doi.org/10.3390/mps3010019.

Guérin, G., Mercier, N., Adamiec, G., 2011. Dose-rate conversion factors: update. AncientTL 29, 5–8.

Hanesch, M., Scholger, R., 2005. The influence of soil type on the magnetic susceptibility measured throughout soil profiles. Geophys. J. Int. 161, 50–56. https://doi.org/10.1111/j.1365-246X.2005.02577.x.

Hanson, P.R., Mason, J.A., Jacobs, P.M., Young, A., 2015. Evidence for bioturbation ofluminescence signals in eolian sand on upland ridgetops, southeastern Minnesota, USA. Quat. Int. 362, 108–115. https://doi.org/10.1016/j.quaint.2014.06.039.

Hatté, C., Gauthier, C., Rousseau, D.-D., Antoine, P., Fuchs, M., Lagroix, F., Markovich, S. B., Moine, O., Sima, A., 2013. Excursions to C_4 vegetation recorded in the Upper Pleistocene loess of Surduk (Northern Serbia): an organic isotope geochemistry study. Clim. Past 9, 1001–1014. https://hal.archives-ouvertes.fr/hal-01092199.

Hu, P., Liu, Q., Heslop, D., Roberts, A.P., Jin, C., 2015. Soil moisture balance and magnetic enhancement in loess–paleosol sequences from the Tibetan Plateau and Chinese Loess Plateau. Earth Planet. Sci. Lett. 409, 120–132. https://doi.org/10.1016/j.epsl.2014.10.035.

Jacobs, P.M., Mason, J.A., 2007. Late Quaternary climate change, loess sedimentation, and soil profile development in the central Great Plains: a pedosedimentary model. Geol. Soc. Am. Bull. 119, 462–475. https://doi.org/10.1130/B25868.1.

Johnson, W.C., Willey, K.L., 2000. Isotopic and rock magnetic expression of environmental change at the Pleistocene-Holocene transition in the central Great Plains. Quat. Int. 67, 89–106. https://doi.org/10.1016/S1040-6182(00)00011-2.

Johnson, M.O., Mudd, S.M., Pillans, B., Spooner, N.A., Keith Fifield, L., Kirkby, M.J., Gloor, M., 2014. Quantifying the rate and depth dependence of bioturbationbased on optically-stimulated luminescence (OSL) dates and meteoric 10Be. Earth Surf. Process. Landf. 39, 1188–1196.

Jordanova, D., Jordanova, N., 2020. Diversity and peculiarities of soil formation in eolian landscapes – Insights from the mineral magnetic records. Earth Planet. Sci. Lett. 531, 115956. https://doi.org/10.1016/j.epsl.2019.115956.

Jordanova, D., Jordanova, N., 2021. Updating the significance and paleoclimate implications of magnetic susceptibility of Holocene loessic soils. Geoderma 391 (2021), 114982. https://doi.org/10.1016/j.geoderma.2021.114982.

Kemp, R.A., 2001. Pedogenic modification of loess: significance for palaeoclimatic reconstructions. Earth-Sci. Rev. 54, 145–156. https://doi.org/10.1016/S0012-8252(01)00045-9.

Kemp, R.A., Derbyshire, E., Meng, X.M., Chen, F.H., Pan, B.T., 1995. Pedosedimentary reconstruction of a thick loess-paleosol sequence near Lanzhou in north-Central China. Quat. Res. 43, 30–45. https://doi.org/10.1006/qres.1995.1004.

Khider, D., Ahn, S., Lisiecki, L.E., Lawrence, C.E., Kienast, M., 2017. The role of uncertainty in estimating lead/lag relationships in marine sedimentary archives: a case study from the tropical Pacific. Paleoceanography 32, 1275–1290. https://doi.org/10.1002/2016PA003057.

Lai, Z.P., Wintle, A.G., 2006. Locating the boundary between the Pleistocene and the Holocene in Chinese loess using luminescence. Holocene 16, 893–899. https://doi.org/10.1191/0959683606hol980rr.

Landais, A., Capron, E., Masson-Delmotte, V., Toucanne, S., Rhodes, R.H., Popp, T., Vinther, B., Minster, B., Prié, F., 2018. Ice core evidence for decoupling between midlatitudeatmospheric water cycle and Greenland temperature during the last deglaciation. Clim. Past 14, 1405–1415. https://doi.org/10.5194/cp-14-1405-2018.

Lapp, T., Kook, M., Murray, A.S., Thomsen, K.J., Buylaert, J.-P., Jain, M., 2015. A new luminescence detection and stimulation head for the Risø TL/OSL reader. Radiat. Meas. 81, 178–184. https://doi.org/10.1016/j.radmeas.2015.02.001.

Lawrence, C., Harden, J., Maher, K., 2014. Modeling the influence of organic acids on soil weathering. Geochim. Cosmochim. Acta 139, 487–507.

Lee, J.A., Gill, T.E., 2015. Multiple causes of wind erosion in the Dust Bowl. Aeolian Res. 19 (Part A), 15–36. https://doi.org/10.1016/j.aeolia.2015.09.002.

Lehmkuhl, F., Nett, J.J., Pötter, S., Schulte, P., Sprafke, T., Jary, Z., Antoine, P., Wacha, L., Wolf, D., Zerboni, A., Hošek, J., Marković, S.B., Obreht, I., Sümegi, P., Veres, D., Zeeden, C., Boemke, B., Schaubert, V., Viehweger, J., Hambach, U., 2021. Loess landscapes of Europe–Mapping, geomorphology, and zonal differentiation. Earth Sci. Rev. 103496 https://doi.org/10.1016/j.earscirev.2020.103496.

Li, Y., Shi, W., Aydin, A., Beroya-Eitner, M.A., Gao, G., 2020. Loess genesis and worldwide distribution. Earth Sci. Rev. 201, 102947. https://doi.org/10.1016/j.earscirev.2019.102947.

Lin, Y., Hibbert, F.D., Whitehouse, P.L., Woodroffe, S.A., Purcell, A., Shennan, I., Bradley, S.L., 2021. A reconciled solution of Meltwater Pulse 1A sources using sea-level fingerprinting. Nat. Commun. 12, 2015. https://doi.org/10.1038/s41467-021-21990-y (2021).

Liu, Q., Banerjee, S.K., Jackson, M.J., Chen, F., Pan, Y., Zhu, R., 2004. Determining the climatic boundary between the Chinese loess and palaeosol: evidence from aeolian coarse-grained magnetite. Geophys. J. Int. 156 (2), 267–274. https://doi.org/10.1111/j.1365-246X.2003.02148.x.

Longman, J., Veres, D., Ersek, V., Salzmann, U., Hubay, K., Bormann, M., Wennrich, V., Schäbitz, F., 2017. Periodic input of dust over the Eastern Carpathians during the Holocene linked with Saharan desertification and human impact. Clim. Past 13, 897–917. https://doi.org/10.5194/cp-13-897-2017.

Lu, H., Stevens, T., Yi, S., Sun, X.F., 2006. An erosional hiatus in Chinese loess sequences revealed by closely spaced optical dating. Chin. Sci. Bull. 51, 2253–2259. https://doi.org/10.1007/s11434-006-2097-x.

Lu, H., Yi, S., Liu, Z., Mason, J.A., Jiang, D., Cheng, J., Stevens, T., Xu, Z., Zhang, E., Jin, L., Zhang, Z., Guo, Z., Wang, Y., Otto-Bliesner, B., 2013. Variation of East Asian monsoon precipitation during the past 21 k.y. and potential CO2 forcing. Geology 41, 1023–1026. https://doi.org/10.1130/G34488.1.

Magyari, E.K., Pál, I., Vincze, I., Veres, D., Jakab, G., Braun, M., Szalai, Z., Szabó, Z., Korponai, J., 2019. Warm Younger Dryas summers and early late glacial spread of temperate deciduous trees in the Pannonian Basin during the last glacial termination (20-9 kyrcal BP). Quat. Sci. Rev. 225, 105980. https://doi.org/10.1016/j.quascirev.2019.105980.

Maher, B.A., Thompson, R., 1994. Pedogenesis and paleoclimate. Interpretation of the magnetic susceptibility record of Chinese loess-paleosol sequences. Geology 22, 857–859. https://doi.org/10.1130/0091-7613(1993)021%3C1011:PAPIOT%3E2.3.CO;2.

Maher, B., Thompson, R., 1995. Paleorainfall reconstruction from pedogenic magnetic susceptibility variations in the Chinese loess and paleosols. Quat. Res. 44, 383–391. https://doi.org/10.1006/qres.1995.1083.

Maher, B.A., MengYu, H., Roberts, H.M., Wintle, A.G., 2003. Holocene loess accumulation and soil development at the western edge of the Chinese Loess Plateau: implications for magnetic proxies of palaeorainfall. Quat. Sci. Rev. 22, 445–451. https://doi.org/10.1016/S0277-3791(02)00188-9.

Marković, S.B., Timar-Gabor, A., Stevens, T., Hambach, U., Popov, D., Tomić, N., Obreht, I., Jovanović, M., Lehmkuhl, F., Kels, H., Marković, R., Gavrilov, M.B., 2014. Environmental dynamics and luminescence chronology from the Orlovat loess-palaeosol sequence (Vojvodina, northern Serbia). J. Quat. Sci. 29, 189–199. https://doi.org/10.1002/jqs.2693.

Marković, S.B., Stevens, T., Kukla, G., Hambach, U., Fitzsimmons, K., Gibbard, P., Buggle, B., Zech, M., Guo, Z., Hao, Q., Wu, H., O'Hara Dhand, K., Smalley, I., Újvári, G., Sümegi, P., Timar-Gabor, A., Veres, D., Sirocko, F., Vasiljevic, D.A., Jary, Z., Svensson, A., Jović, V., Lehmkuhl, F., Kovács, J., Svirčev, Z., 2015. Danube loess stratigraphy-towards a pan-European loess stratigraphic model. Earth-Sci. Rev. 148, 228–258. https://doi.org/10.1016/j.earscirev.2015.06.005.

Marković, S.B., Sümegi, P., Stevens, T., Schaetzl, R.J., Obreht, I., Chu, W., Buggle, B., Zech, M., Zech, R., Zeeden, C., Gavrilov, M.B., Perić, Z., Svirčev, Z., Lehmkuhl, F., 2018. The Crvenka loess-paleosol sequence: a record of continuous grassland domination in the southern Carpathian Basin during the Late Pleistocene. Palaeogeogr.Palaeoclimatol.Palaeoecol. 509, 33–46.

Mason, J.A., Jacobs, P.M., Hanson, P.R., Miao, X., Goble, R.J., 2003. Sources and paleoclimatic significance of Holocene Bignell loess, central Great Plains, USA. Quat. Res. 60, 330–339. https://doi.org/10.1016/j.yqres.2003.07.005.

Mason, J.A., Miao, X.D., Hanson, P.R., Johnson, W.C., Jacobs, P.M., Goble, R.J., 2008. Loess record of the Late Pleistocene to Holocene transition on the central and northern Great Plains. Quat. Sci. Rev. 27, 1772–1783. https://doi.org/10.1016/j.quascirev.2008.07.004.

McDonald, E.V., Busacca, A.J., 1990. Interaction between aggrading geomorphic surface and the formation of a Pleistocene paleosol in the Palouse Loess of eastern Washington state. Geomorphology 3, 449–469. https://doi.org/10.1016/0169-555X(90)90016-J.

Mejdahl, V., 1979. Thermoluminescence dating: beta-dose attenuation in quartz grains. Archaeometry 21, 61–72. https://doi.org/10.1111/j.1475-4754.1979.tb00241.x.

Miao, X., Xulong, W., Mason, J.A., 2006. Isolation of the syndepositional magnetic susceptibility signals from loessic paleosols of China. J. Asian Earth Sci. 27 (5), 684–690. https://doi.org/10.1016/j.jseaes.2005.06.007.

Miao, X.D., Mason, J.A., Johnson, W.C., Wang, H., 2007. High-resolution proxy record of Holocene climate from a loess section in Southwestern Nebraska, USA. Palaeogeogr. Palaeoclimatol. Palaeoecol. 245, 368–381. https://doi.org/10.1016/j.palaeo.2006.09.004.

Miao, X., Wang, H., Hanson, P., Mason, J., Liu, X., 2015. A new method to constrain soil development time using both OSL and radiocarbon dating. Geoderma 261, 93–100. https://doi.org/10.1016/j.geoderma.2015.07.004.

Muhs, D.R., McGeehin, J.P., Beann, J., Fisher, E., 2004. Holocene loess deposition and soil formation as competing processes, Matanuska Valley, Southern Alaska. Quat. Res. 61 (03), 265–276. https://doi.org/10.1016/j.yqres.2004.02.003.

Murray, A.S., Wintle, A.G., 2000. Luminescence dating of quartz using an improved single-aliquot regenerative-dose protocol. Radiat. Meas. 32, 57–73. https://doi.org/10.1016/S1350-4487(99)00253-X.

Murray, A.S., Wintle, A.G., 2003. The single aliquot regenerative dose protocol: potential for improvements in reliability. Radiat. Meas. 37, 377–381. https://doi.org/10.1016/S1350-4487(03)00053-2.

Nawrocki, J., Bakhmutov, V., Bogucki, A., Dolecki, L., 1999. The paleo- and petromagnetic record in the polish and Ukrainian loess-palaeosol sequences. Phys. Chem. Earth A 24 (9), 773–777. https://doi.org/10.1016/S1464-1895(99)00113-1.

Necula, C., Dimofte, D., Panaiotu, C., 2015. Rock magnetism of a loess-palaeosol sequence from the western Black Sea shore (Romania). Geophys. J. Int. 202 (3), 1733–1748. https://doi.org/10.1093/gji/ggv250.

Orgeira, M.J., Compagnucci, R.H., 2006. Correlation between paleosol-soil magnetic signal and climate. Earth Planets Space 58, 1373–1380. https://doi.org/10.1186/BF03352633.

Orgeira, M.J., Egli, R., Compagnucci, R.H., 2011. A quantitative model of magnetic enhancement in loessic soils. Earth's Mag. Int. 1, 361–397. https://doi.org/10.1007/978-94-007-0323-0_25.

Panaiotu, C.G., Panaiotu, E.C., Grama, A., Necula, C., 2001. Paleoclimatic record from a loess–paleosol profile in Southeastern Romania. Phys.Chem.Earth.(A) 26, 893–898. https://doi.org/10.1016/S1464-1895(01)00138-7.

Prescott, J.R., Hutton, J.T., 1994. Cosmic ray contributions to dose rates for luminescence and ESR dating: large depths and long term variations. Radiat. Meas. 23, 497–500. https://doi.org/10.1016/1350-4487(94)90086-8.

Rasmussen, S.O., Bigler, M., Blockley, S.P., Blunier, T., Buchardt, S.L., Clausen, H.B., Cvijanovic, I., Dahl-Jensen, D., Johnsen, S.J., Fischer, H., Gkinis, V., Guillevic, M., Hoek, W.Z., Lowe, J.J., Pedro, J.B., Popp, T., Seierstad, I.K., Steffensen, J.P., Svensson, A.M., Vallelonga, P., Vinther, B.M., Walker, M.J.C., Wheatley, J.J., Winstrup, M., 2014. A stratigraphic framework for abrupt climatic changes during the last Glacial period based on three synchronized Greenland ice-core records: refining and extending the INTIMATE event stratigraphy. Quat. Sci. Rev. 106, 14–28. https://doi.org/10.1016/j.quascirev.2014.09.007.

Rees-Jones, J., 1995. Optical dating of young sediments using fine-grain quartz. Ancient TL 13, 9–13.

Roberts, H.M., 2008. The development and application of luminescence dating to loess deposits: a perspective on the past, present and future. Boreas 37, 483–507. https://doi.org/10.1111/j.1502-3885.2008.00057.x.

Roberts, H.M., Muhs, D.R., Wintle, A.G., Duller, G.A.T., Bettis III, E.A., 2003. Unprecedented last glacial mass accumulation rates determined by luminescence dating of loess from western Nebraska. Quat. Res. 59, 411–419. https://doi.org/10.1016/S0033-5894(03)00040-1.

Rousseau, D.D., Boers, N., Sima, A., Svensson, A., Bigler, M., Lagroix, F., Taylor, S., Antoine, P., 2017. (MIS3 & 2) millennial oscillations in Greenland dust and Eurasian aeolian records – a paleosol perspective. Quat. Sci. Rev. 169, 99–113. https://doi.org/10.1016/j.quascirev.2017.05.020.

Rousseau, D.D., Antoine, P., Sun, Y., 2021. How dusty was the last glacial maximum over Europe? Quat. Sci. Rev. 254, 106775. https://doi.org/10.1016/j.quascirev.2020.106775.

Schaetzl, R., Anderson, A., 2009. Soils. In: Genesis and Geomorphology. Cambridge Univ. Press, UK. ISBN978-0-521-81201-6.

Schaetzl, R.J., Bettis, E.A., Crouvic, O., Fitzsimmons, K.E., Grimley, D.A., Hambach, U., Lehmkuhl, F., Markovic, S.B., Mason, J.A., Owczarek, P., Roberts, H.M., Rousseau, D.D., Stevens, T., Vandenberghe, J., Zarate, M., Veres, D., Yang, S.L., Zech, M., Conroy, J.L., Dave, A.K., Faust, D., Hao, Q.Z., Obreht, I., Prud'homme, C., Smalley, I., Tripaldi, A., Zeeden, C., Zech, R., 2018. Approaches and challenges to the study of loess - introduction to the Loess-Fest. Quat. Res. 89, 563–618. https://doi.org/10.1017/qua.2018.15.

Song, Y., Hao, Q., Ge, J., Zhao, D., Zhang, Y., Li, Q., Zuo, X., Lü, Y., Wang, P., 2014. Quantitative relationships between magnetic enhancement of modern soils and climatic variables over the Chinese Loess Plateau. Quat. Int. 334–335, 119–131. https://doi.org/10.1016/j.quaint.2013.12.010.

Stern, J.V., Lisiecki, L.E., 2014. Termination 1 timing in radiocarbon-dated regional benthic $\delta^{18}O$ stacks. Paleoceanography 29, 1127–1142. https://doi.org/10.1002/2014PA002700.

Stevens, T., Armitage, S.J., Lu, H., Thomas, D.S.G., 2006. Sedimentation and diagenesis of Chinese loess: implications for the preservation of continuous, high-resolution climate records. Geology 34 (10), 849–852. https://doi.org/10.1130/G22472.1.

Stevens, T., Thomas, D.S.G., Armitage, S.J., Lunn, H.R., Lu, H., 2007. Reinterpreting climateproxy records from late Quaternary Chineseloess: a detailed OSL investigation: EarthSci. Rev. 80, 111–136. https://doi.org/10.1016/j.earscirev.2006.09.001.

Stevens, T., Lu, H., Thomas, D.S.G., Armitage, S.J., 2008. Optical dating of abrupt shifts in the late Pleistocene East Asian monsoon. Geology 36 (5), 415–418. https://doi.org/10.1130/G24524A.1.

Stevens, T., Marković, S.B., Zech, M., Hambach, U., Sümegi, P., 2011. Dust deposition and climate in the Carpathian Basin over an independently dated last glacial-interglacial cycle. Quat. Sci. Rev. 30, 662–681. https://doi.org/10.1016/j.quascirev.2010.12.011.

Sun, J.M., Zhang, M.Y., Liu, T.S., 2001. Spatial and temporal characteristics of duststorms in China and its surrounding regions, 1960-1999: relations to sourcearea and climate. J. Geophys. Res.-Atmos. 106 https://doi.org/10.1029/2000JD900665, 10325e10333.

Tecsa, V., Gerasimenko, N., Veres, D., Hambach, U., Lehmkuhl, F., Schulte, P., Timar-Gabor, A., 2020a. Revisiting the chronostratigraphy of late Pleistocene loess-paleosolsequences in southwestern Ukraine: OSL dating of Kurortnesection. Quat. Int. 542, 65–79. https://doi.org/10.1016/j.quaint.2020.03.001.

Tecsa, V., Mason, J.A., Johnson, W.C., Miao, X., Constantin, D., Radu, S., Magdas, D.A., Veres, D., Marković, S.B., Timar-Gabor, A., 2020b. Late Pleistocene to Holocene loess in the central Great Plains: Optically stimulated luminescence dating and multi-proxy analysis of the Enders section (Nebraska, USA). Quat. Sci. Rev. 229, 106130. https://doi.org/10.1016/j.quascirev.2019.106130.

Timar-Gabor, A., Constantin, D., Marković, S., Jain, M., 2015. Extending the area of investigation of fine versus coarse quartz optical ages on Serbian loess. Quat. Int. 388, 168–176. https://doi.org/10.1016/j.quaint.2014.09.065.

Újvári, G., Kok, J.F., Varga, G., Kovács, J., 2016. The physics of wind-blown loess: Implications for grain size proxy interpretations in Quaternary paleoclimate studies. Earth-Sci. Rev. 154, 247–278. https://doi.org/10.1016/j.earscirev.2016.01.006.

Vandenberghe, D.A.G., De Corte, F., Buylaert, J.-P., Kučera, J., Van den Haute, P., 2008. On the internal radioactivity in quartz. Radiat. Meas. 43, 771–775. https://doi.org/10.1016/j.radmeas.2008.01.016.

Walker, M., Head, M.J., Lowe, J., Berkelhammer, M., Björck, S., Cheng, H., Cwynar, L., Fisher, D., Gkinis, V., Long, A., Lowe, J., Newnham, R., Rasmussen, S., Weiss, H., 2019. Subdividing the Holocene Series/Epoch: formalization of stages/ages and subseries/subepochs, and designation of GSSPs and auxiliary stratotypes. J. Quat. Sci. 34, 173–186. https://doi.org/10.1002/jqs.3097.

Zeeden, C., Dietze, M., Kreutzer, S., 2018. Discriminating luminescence age uncertainty composition for a robust Bayesian modelling. Quat.Geochronol. 43, 30–39. https://doi.org/10.1016/j.quageo.2017.10.001.

Zeeden, C., Obreht, I., Veres, D., Kaboth-Bahr, S., Hošek, J., Marković, S.B., Bösken, J., Lehmkuhl, F., Rolf, C., Hambach, U., 2020. Smoothed millennial-scale palaeoclimaticreference data as unconventional comparison targets: application to European loess records. Sci. Rep. 10, 5455. https://doi.org/10.1038/s41598-020-61528-8.